

# Connection between microbiome and neurodegenerative diseases: how microbiota-derived prions can affect development of Alzheimer's disease

---

Tić, Iva

Master's thesis / Diplomski rad

2022

Degree Grantor / Ustanova koja je dodijelila akademski / stručni stupanj: **University of Rijeka / Sveučilište u Rijeci**

Permanent link / Trajna poveznica: <https://um.nsk.hr/um:nbn:hr:193:119946>

Rights / Prava: [In copyright](#) / [Zaštićeno autorskim pravom.](#)

Download date / Datum preuzimanja: **2024-05-19**

Repository / Repozitorij:



[Repository of the University of Rijeka, Faculty of Biotechnology and Drug Development - BIOTECHRI Repository](#)



UNIVERSITY OF RIJEKA  
DEPARTMENT OF BIOTECHNOLOGY  
Master's degree  
"Research and drug development"

Iva Tić

**CONNECTION BETWEEN MICROBIOME AND NEURODEGENERATIVE  
DISEASES: HOW MICROBIOTA-DERIVED PRIONS CAN AFFECT  
DEVELOPMENT OF ALZHEIMER'S DISEASE**

Master thesis

Mentor: dr. Natalia Sanchez de Groot,  
Comentor: doc. dr. sc. Željka Minić

**Rijeka, 2022**

SVEUČILIŠTE U RIJECI  
ODJEL ZA BIOTEHNOLOGIJU  
Diplomski studij  
"Istraživanje i razvoj lijekova"

Iva Tić

**POVEZANOST MIKROBIOMA I NEURODEGENERATIVNIH BOLESTI:  
KAKO PRIONI IZOLIRANI IZ MIKROBIOMA UTJEČU NA RAZVOJ  
ALZHEIMEROVE BOLESTI**

Diplomski rad

Mentor: dr. Natalia Sanchez de Groot,

Komentor: doc. dr. sc. Željka Minić

**Rijeka, 2022.**

Master thesis defended on 26/09/2022 in front of committee:

1. doc. dr. sc. Christian Andrew Reynolds
2. dr. sc. Elitza Petkova Markova Car
3. doc. dr.sc. Željka Minić

Thesis has 49 pages, 11 figures, 4 tables and 56 literature citations

## **ACKNOWLEDGEMENT**

I would like to thank my mentor Natalia Sanchez de Groot for giving me the opportunity to work on this project and for all time and effort she put in guiding me in her laboratory while fully believing in my laboratory skills. I am very grateful to Maria Rosario Fernández Gallegos as well for the help, kindness, and everything that she taught me about the yeast system in previous 6 months.

Thanks go to my family for their support and patience during all these years of education.

## **ABSTRACT**

The idea that Alzheimer's disease (AD) has an origin in the gut has been widely accepted based on crosstalk between microbiota, gut and brain. To the hypothesis of the present work, gut microbiota could be a source of a major number of amyloids. This work used two of the best studied bacterial amyloids; (i) curli, produced by *Escherichia coli* and (ii) Sup35p, produced by *Saccharomyces cerevisiae*. Curli has beneficial roles for bacteria by helping them to form biofilms and to resist destruction by physical or immune factors, while at the same time share similarities inside tertiary structure with central nervous system's (CNS) amyloids that are responsible for forming toxic A $\beta$  plaques in AD. Under certain circumstances bacterial derived amyloids can leak from GI tract and accumulate at the systemic and brain level. In order to discern which peptides from human microbiome are able to influence human proteins aggregation, this work implemented proteome-wide bioinformatic tools and *in vitro* assays to follow which putative amyloid core sequence can lead the formation of amyloid aggregates and the cell-to-cell transmission of the aggregated conformation. Production of amyloid fibrils through CDAG system based on curli was achieved with all 12 tested peptides and their existence was proved by phenotype evaluation in the liquid and on plates containing the amyloid binding dye (Congo red, CR) as well as under Transmission electron microscopy (TEM). The Sup35p prion system, that regulates translation termination in *Saccharomyces cerevisiae* was used to test the ability of the amyloid cores, to propagate the amyloid aggregated conformation between yeast cells. Finally, bacterial and yeast systems provided simplified models for studying the conserved mechanisms of amyloid formation, degradation, and function as well as connection between bacterial amyloids and amyloid structures in brain formed during neurodegeneration.

## **KEY WORDS**

bacterial amyloids, prion-like peptides, curli, CDAG- system, Sup35p

## SAŽETAK

Unatrag nekoliko godina povezanost intestinalnog sustava s nastankom neurodegenerativnih bolesti kao što je Alzheimer postaje sve istraženije područje temeljeno na komunikaciji između mozga i crijevnog sustava te crijevnog mikrobioma. Prema hipotezi ovog rada, crijevni mikrobiom čini potencijalni rezervoar velike količine amiloida. Shodno tome, u ovom radu su korištena dva najbolje proučena amiloida; (i) curli, koje proizvodi *Escherichia coli* te (ii) Sup35p, koje proizvodi *Saccharomyces cerevisiae*. Curli imaju korisnu ulogu u formiranju bakterijskog biofilma i zaštiti od fizičkih ili imunoloških oštećenja stanice, dok istovremeno dijele sličnosti s tercijskom strukturom amiloida koji se nakupljaju u središnjem živčanom sustavu čineći toksične A $\beta$  plakove- jedne od glavnih patoloških markera Alzheimerove bolesti. Pod određenim okolnostima amiloidi bakterijskog podrijetla mogu „curiti“ iz gastrointestinalnog (GI) trakta i akumulirati se u mozgu. Kako bi se razlučilo koji peptidi izolirani iz ljudskog mikrobioma mogu utjecati na agregaciju ljudskih proteina, ovaj rad implementirao je bioinformatičke alate za analizu cijelog proteoma te *in vitro* ispitivanja kako bi se utvrdilo koja sekvenca amiloidne jezgre može dovesti do stvaranja amiloidnih nakupina i prijenosa agregiranih konformacija s jedne na drugu stanicu. Proizvodnja amiloidnih fibrila putem CDAG sustava postignuta je kod svih 12 testiranih peptida, a njihov potencijal je dokazan procjenom fenotipa na mikrobiološkim pločama i u tekućini koje sadrže boju za vezanje amiloida (engl. Congo red, CR). Proizvodnja amiloidnih agregata je također vizualizirana transmisijom elektronskom mikroskopijom (TEM). Sup35p prionski sustav, koji regulira prekid translacije u *Saccharomyces cerevisiae*, korišten je za testiranje sposobnosti amiloidnih jezgri da propagiraju amiloidne nakupine između stanica kvasca. Zaključno, sustavi bakterija i kvasca omogućili su proučavanje očuvanih mehanizama stvaranja, razgradnje i funkcije amiloida te promaknuli saznanja o povezanosti bakterijskih amiloida s amiloidnim formacijama koje nastaju tijekom neurodegeneracije.

## **KLJUČNE RIJEČI**

bakterijski amiloidi, prion-nalik proteini, CDAG sustav, curli, Sup35p



## TABLE OF CONTENTS

1. INTRODUCTION.....	1
1.1. Alzheimer’s disease.....	1
1.2. Prions and prion-like proteins.....	3
1.2.1. Amyloid fibrils and protofibrils.....	4
1.3. Identification of novel human prion like proteins.....	5
1.3.1. Computational analysis .....	5
1.4. Gut-brain axis .....	6
1.4.1. Microbiome impact on amyloidosis.....	6
1.5. Prion behavior in the yeast model.....	7
1.6. Sup35p protein .....	8
1.6.1. Sup35p in <i>E. coli</i> and <i>S. cerevisiae</i> models .....	10
1.7. CDAG system in <i>E. coli</i> .....	11
1.7.1. Curli fibers- functional amyloids .....	12
2. AIM OF THE WORK.....	14
3. MATHERIALS AND METHODS .....	15
3.1. Putative prion-like peptides.....	15
3.2. Escherichia coli system.....	17
3.2.1. Strains, growth condition and cultivation .....	17
3.2.2. Plasmid isolation, purification, and transformation .....	18
3.2.3. Congo red (CR) binding assay .....	20
3.2.4. Transmission electron microscopy (TEM) .....	21
3.3. Analysis of prion behavior in <i>Saccharomyces cerevisiae</i> .....	21
3.3.1 Endogenous expression of Sup35p chimeres and plasmid shuffling .....	23
3.3.2. Overexpression of NM-P9 fused to GFP.....	24
3.3.3. Phenotypic assay.....	26
3.3.4. Western blot analysis.....	26
4. RESULTS.....	28
4.1. Production of curli.....	28
4.1.1. Congo red phenotypic assay- plates.....	28
4.1.2. Congo red phenotypic assay- liquid.....	30
4.1.3. Curli fibers characterization .....	31

4.2. Analysis of peptide 9 prion behavior in the yeast model .....	34
5. DISCUSSION .....	37
5.1. Production of curli .....	37
5.2. Transmission of the aggregated conformations in yeast .....	39
6. CONCLUSION .....	42
7. LITERATURE .....	43
8. CURRICULUM VITAE .....	49

## **1. INTRODUCTION**

Since 2009, when the composition of the human microbiome ( $\sim 10^{13}$  microbial cells) was published (1), researchers have made great progress in the revelation of its good influence on human health. At the same time, alterations in a healthy microbiome have been observed and connected with neurodegeneration. Particularly, there is an increasing number of research that hypothesize about connections between gut microbiota and the development of amyloid aggregates in the brain. For now, gastrointestinal (GI) tract has been implicated in several neurological disorders such as autism spectrum disorder, anxiety, and depression, while microbiota is increasingly recognized for its ability to affect the development and function of the nervous system. It is due to the bidirectional network called gut-brain axis that interconnects the gut and brain under the control of gut microbiota. Crosstalk between human's and microbiome's amyloids is now in the focus because it seems like host proteins may be triggered to aggregate by the influence of amyloids produced by gut microorganisms. Furthermore, published literature supports the idea that Alzheimer's disease (AD) has an origin in the gut. This is based on observational experiments with AD patients that show different gut microbiome composition when compared to healthy patients (2).

### **1.1. Alzheimer's disease**

AD is a degenerative brain disease and the most common form of dementia characterized by large amounts of amyloid plaques surrounded by neurons (3). According to the Alzheimer's Association, worldwide, at least 50 million people are believed to be suffering from AD or other dementias (4). AD is the most frequent type of amyloidosis in humans and is very well described in published literature. Also, other neurodegenerative diseases such as Parkinson's and Huntington's disease have a source in depositions of amyloids that are highly organized cross- $\beta$ -sheet-rich protein aggregates. More precisely they display fibrillar structure, which is

constituted by repetitions of a specific protein in  $\beta$ -sheet conformation packed perpendicular to the fibril axis (Figure 1a) (5). Importantly, the formation of cross  $\beta$ -sheet rich structure is largely independent of the amino acid sequence and native fold of the protein of which the fibrils are composed (6).

A widely accepted hypothesis, also known as “The amyloid cascade hypothesis”, relies on the deposition of the amyloid- $\beta$  peptide ( $A\beta$ ) in the brain parenchyma which initiates a sequence of events such as cell loss, neurofibrillary tangles and vascular damage that will, in the end, lead to AD dementia (7).  $A\beta$  is the most extensively characterized amyloid fibril, and it is formed from Amyloid protein precursor (APP) when its cleavage happens with  $\beta$ -secretase instead of  $\alpha$ -secretase (1). Further developments in this area of research point out that different neurodegenerative diseases have common cellular and molecular mechanisms, including protein aggregation and inclusion body formation.

Since the year of 2002 it is evident that the ability to form amyloid fibrils is an inherent property of polypeptides and there are certain *in vitro* conditions under which peptides and proteins with no connection with a disease can convert into fibrils and protofibrils with same characteristics as those associated with amyloid disorders (8).

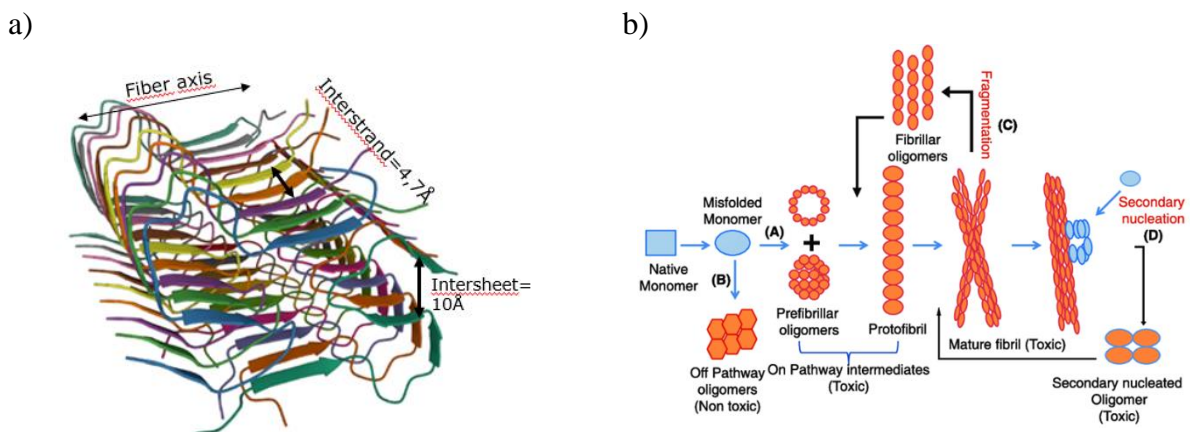


**Figure 1. a) Atomic Resolution Structure of Monomorphic  $A\beta_{42}$  Amyloid Fibrils.** Arrows indicate interstrand and intersheet distances. **b) Formation of fibrils in four aggregation pathways** (9,10).

## **1.2. Prions and prion-like proteins**

Prions are defined as proteins (subclass of amyloids) that convert between structurally and functionally distinct states, at least one of which is self-propagating and self-perpetuating (11). In that way, they possess an ability to spread a structural conformation, usually an amyloid structure, to other proteins even across species. Their phenotypic variations can be inherited following a non-Mendelian pattern, while their manifestation relies on the interactions of multiple copies of a protein under specific conditions. Besides, this mechanism of the epigenetic transmission of information differs significantly from DNA based inheritance. In Creutzfeldt-Jakob disease, the development of prions occurs during the aberrant folding of a cellular protein (PrP<sup>C</sup>) into an infectious “scrapie” form (PrP<sup>Sc</sup>). This conformational change has relation with its transmissibility, the ability to promote the conversion of the normally folded protein into a prion isoform, although the functions of the endogenous prion protein are still unknown (12).

It is important to emphasize that all prions are amyloids but not all amyloids are prions. Despite the overlapping conformational properties, only a small number of amyloids have shown a prions transmissibility behavior in native conditions (13). Usually, amyloid proteins contain specific regions rich in hydrophobic residues that lead the protein self-assembly, while prion-like proteins exhibit domains that are often enriched in asparagine and glutamine (Q/N), creating low complexity regions (LCR) (14). These LCR exhibit disordered structures, a crucial property that ensures conformational flexibility and self-assembly (15). Another characteristic of prions is their reversible nature, which gives an opportunity for their recovery.

Prions were being studied mainly in mammals while the presence of prion-like domains and prion-like proteins has been discovered in organisms of all kingdoms of life, including viruses (16). Even if they are associated to many physiological and pathological processes, sometimes may have a

beneficial role for living species in generating novel and diverse biological functions. Furthermore, it seems that fungi's (especially yeast) prions have an important role in epigenetic inheritance. Their conformational switch can cause functional and phenotypic changes without changes at nucleic acid level.

### ***1.2.1. Amyloid fibrils and protofibrils***

As mentioned before, amyloids appear in unbranched and highly stable structures, with a size of few nanometers in diameter. They are composed of several protofilaments that wrap each other around. These protofibrils (4-11 nm in diameter) are prefibrillar entities that results in the formation of mature amyloid fibrils, in this process monomers are added to grow the oligomeric chain (Figure 1b). However, those assemblies have been found in many diseases associated proteins as well in proteins not associated with amyloidosis (17). Lately, published literature emerged with new evidence about the toxicity of prefibrillar species, especially oligomers, formed during early fibrillization. Their results show a higher toxic rate compared to the mature fibrils (18). Main difference is that mature amyloid fibers are consisted of parallel  $\beta$ -sheets, while antiparallel conformations of  $\beta$ -strands are mainly represented in protofibrils. Variability of parallel and antiparallel  $\beta$ -structures were also detected in A $\beta$ -amyloid and prion-related peptides. Controversially, the formation of mature fibrils is believed to be protective because they serve as a reservoir of toxic oligomers, but they can also result in their releasement and production of toxic outcome. Apparently, the amyloid cascade hypothesis has been modified to include the intermediary species formed during the aggregation process. Oligomers are relatively small in size, so can diffuse easier through tissues if compared to larger fibrils. Furthermore, they possess a higher number of open active ends what enables better interactions with cellular targets. So, the literature supports the idea that the differential toxicity of amyloid oligomers and fibrils is due to their different structural arrangements (19). Finally, if protofibrils are

produced in the bacterial environment (e.g. in the gut) they can be toxic not only for the host organism but for bacteria as well.

### **1.3. Identification of novel human prion like proteins**

Properties of prion forming domain (PFD) are encoded in the primary sequence of proteins, so identification of prionogenic sequences in genomes can be performed by using different algorithms. First obstacle in designing a prion-like prediction algorithm was the short number of known prions. Some algorithms operate considering that a prion-like domain could be detected just by composition while others are taking into account the amino acid arrangement. Proteome-wide bioinformatics showed that prionic transmissibility relies on intrinsically disordered regions. In these regions, the contact that brings two protein chains at a close distance tends to be weak, abundant, and spread along a sequence or be led by a smaller driver domain or amyloid-forming core.

#### ***1.3.1. Computational analysis***

The algorithms developed to detect prion-like sequences are based on different strategies. Prion Aggregation Prediction Algorithm (PAPA) works on basis of scanning proteins with 81 amino acid window and scores them based on disorder and Q/N rich domains. Regions with a PAPA score above 0.05, indicate a high probability of prion-like sequence. pWALTZ algorithm should work on disorder protein regions and looks for nucleating cores of 21 amino acid residues. It has been proved experimentally that the nucleating regions predicted by pWALTZ can be exchanged between disordered regions of different proteins retaining the ability to lead the aggregation of the whole molecule. Another algorithm is PLAAC which uses a hidden Markov model (HMM) to determine the propensity of an amino acid to be part of a prion-like domain, then scores the prion probability and identifies the most probable prion.

#### **1.4. Gut-brain axis**

Recently, gut-brain crosstalk has been considered as bidirectional and includes a complex communication system that ensures the proper maintenance of gut homeostasis while in the same time effects higher cognitive functions. These two complexes are connected through various routes including tryptophan metabolism, the immune system, the vagus nerve, and the enteric nervous system (ENS), involving microbial metabolites such as peptidoglycans, short-chain fatty acids and branched chain amino acids. Any alteration in gut-brain network can affect gut inflammation disorders, altered responses to acute and chronic stress as well as modified behavioral states (20).

##### **1.4.1. Microbiome impact on amyloidosis**

Many studies suggest that human symbiotic microbes have a big influence on host health since the number of gut colonizing bacteria was revealed and their density was estimated as the highest in any microbial ecosystem. Microbiome contains more than 1000 different bacterial species and outnumbers human genes by 150 times. Among all of them, Bacteroidetes and Firmicutes are two dominant bacterial phyla in the gut. For example, investigators have shown that gut microbiota can affect animal's behavior and be able to change the brain physiology and neural biochemical characteristics after several experiments on germ-free (GF) mice (21,22). They revealed that, if GF mice were colonized with normal gut microbiota from conventionally raised mice or specific probiotic *Bifidobacterium*, infants were able to reverse described abnormalities. On the other hand, under chronic inflammation conditions, the gut microbiome might release high amounts of amyloid-enhancing factors which facilitate a multitude of interactions with the host. *Escherichia coli*, *Salmonella enterica*, *Salmonella typhimurium*, *Bacillus subtilis* and *Staphylococcus aureus* are some of the pathogenic strains that produce functional extracellular amyloid fibers, but they were found also in naturally occurring populations of Proteobacteria, Bacteroidetes and Actinobacteria (23).



Considering the gut role in transmission of prions, it is believed that the GI tract might also play a role in A $\beta$  formation and transmission, consequently leading to the development of AD. There is a hypothesis that explains how gut microbiota is implicated in pathogenesis. Literature supports the idea of leakiness of bacteria-derived amyloids from the gastrointestinal tract and their accumulation at the systemic and brain level (24,25). They explained that these events might cause an increase in reactive oxygen species (ROS) and the activation of nuclear factor- $\kappa$ B (NF- $\kappa$ B) signaling, through upregulating levels of micro RNA-34a (miRNA-34a). As a consequence, miRNA-34a downregulates the expression of “triggering receptor expressed in microglial/myeloid cells-2” (TREM2), leading to impairment of phagocytosis that contributes to the accumulation of A $\beta$ 42 peptide. Furthermore, it increases the levels of cytokines and other small proinflammatory molecules, such as interleukins directly associated with AD. Additionally, microbial amyloids were shown to have a molecular and cellular role in processes like tissue invasion, biofilm development and toxin storage (26). Amyloid cross-seeding events between host and microorganism may be initiated by the long exposure to microorganisms, during the infection or symbiosis.

All in all, it is of great importance to identify the microorganisms and precise mechanisms that are included in the aggregation of host proteins. Those findings will help to design new therapeutic strategies, such as microbiome manipulation with probiotics.

### **1.5. Prion behavior in the yeast model**

After years of investigation, it has been concluded that yeast prions are propagated through generations by transmitting aggregated “seeds” from mother to daughter cells via cytoplasm (27). Researchers have found out that there are few yeast prions that can act as heritable protein-based genetic elements, nonhomologous to each other or to the mammalian prion protein. Yeast prion proteins are characterized by having glutamine/asparagine (Q/N)-rich domains and showing low-complexity

profiles. The most widely studied amyloid-based prions of *Saccharomyces cerevisiae* are: Ure2p, a regulator of nitrogen catabolism; and Sup35p, a subunit of the essential translation termination factor eRF3. In both cases, prion amyloid formation prevents the normal protein function, producing a phenotype with adaptative implications (28). For instance, it has been suggested that under certain stress conditions the aggregation of Sup35p, also called  $[PSI^+]$  phenotype, may be induced to alter translation and improve cell survival under stress. It manifests as a nonfunctional and ordered aggregate of Sup35p and enables other proteins to adopt prionic state. Chaperons are also involved in the induction of the  $[PSI^+]$ . Fragmentation of prion polymers by the Hsp104 chaperone represents a key step of the prion replication cycle.  $[PSI^+]$  can be eliminated by transient growth in the presence of guanidine hydrochloride (GuHCl), which “cures” cells of prions by inhibiting Hsp104p. In the case of the other chaperones, under stress conditions they are occupied dealing with the stress negative effects, thus won’t be able to prevent prion formation and/or replication (28).

### **1.6. Sup35p protein**

In this thesis, the focus will be on Sup35p protein and how its conformational alterations in yeast and bacteria cells produce a prionic phenotype. Sup35p protein is a translation termination factor composed of three domains (Figure 2). The first one is a prionogenic N-terminal domain (N) with 1–123 amino acids (in Figure 2 colored in blue grey) bearing the prion-like domain. It is composed of two distinct regions, of which one is enriched in glycine, glutamine, asparagine, and tyrosine (residues 1-39) and the other one contains five complete copies of an oligopeptide repeat (residues 40–112, Figure 2). The second domain is a middle one (M-yellow) with 124–253 amino acids and it interacts with the Hsp104 chaperone managing solubility of Sup35p and maintaining it in the non-prion form. This one is important for the mitotic stability of the prion. Finally, the C-terminal GTPase domain contains 254–685 amino acids (colored in orange)

and it contributes to translation termination activity, but it is unnecessary for prion behavior. Domains N and M are needed for the formation of stable prions acting as prion-propagation module that is transferable to heterologous proteins. When Sup35p acquires the prion conformation, it assembles into amyloid aggregates and has the ability to recruit new monomers (29).

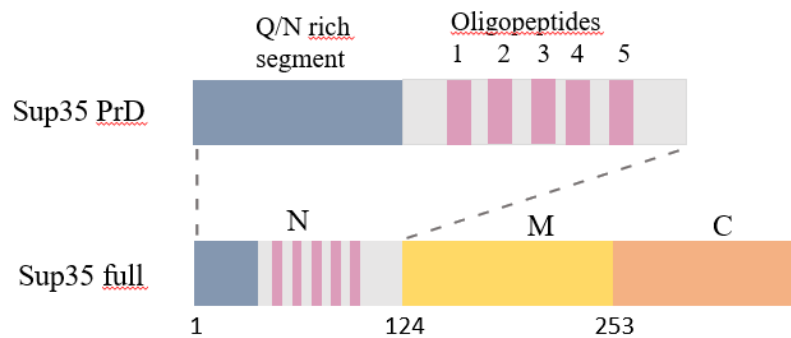


**Figure 2. Sup35p structure.** The N-terminal PrD of Sup35p has two distinct regions that contribute to polymerization of Sup35p and propagation of  $[PSI^+]$ : a Q/N-rich region (QNR; residues 1–40) and an oligopeptide repeat region (OPR; residues 41–97). The OPR is composed of five imperfect peptide repeats (consensus PQGGYQQYN) that are similar in sequence to the octarepeats found in mammalian PrP (PHGGGWGQ) (30).

Under stress, Sup35p structure switches to a prionic conformation, impeding its binding to the stop codon and allowing ribosomes to read through it. Accordingly, strains containing  $[PSI^+]$  form will display a nonsense-suppression phenotype. Upon deletion of the Sup35p prion domain (PrD), Sup35p protein remains soluble and functional even in  $[PSI^+]$  yeast, while the transient overexpression of this domain induces conversion of  $[psi^-]$  yeast to  $[PSI^+]$  (31). *In vivo* validation can be carried out by substituting the PrD from the Sup35p with the soft-amyloid core sequence. When Sup35p aggregates in  $[PSI^+]$  cells, the lack of soluble functional protein leads to a decrease in translation termination efficiency, which can be detected by a non-sense suppressor assay. In this assay, a premature stop codon is present in *ade1-14* gene which inactivates it. Therefore, when

Sup35p is soluble, [*psi*<sup>-</sup>] cells are auxotrophic for adenine and show accumulation of the red metabolite from adenine biosynthesis 5'-P-ribosyl-5-aminoimidazole. In the opposite side, when Sup35p aggregates the premature stop codon can be read-through and [*PSI*<sup>+</sup>] cells can grow without adenine supplementation and become white or pink (Figure 4). The modularity of Sup35p allows the substitution of its N-terminal domain by the soft-amyloid cores, and therefore to assay its ability to induce the [*PSI*<sup>+</sup>] conversion *in vivo*.

According to the current publications, only changes in the middle region of Sup35p have been investigated (32), while existence of the shortened transcript of the Sup35p gene in certain conditions has been reported but never studied carefully. This work intends to explain more precisely how deletion of the first 40 amino acids from the N region of Sup35p and insertion of peptides; which have prionic propensity; would affect phenotype in *E. coli* and *S. cerevisiae*.

#### **1.6.1. Sup35p in *E. coli* and *S. cerevisiae* models**

Sup35p protein, can switch between soluble form [*psi*<sup>-</sup>] which is biochemically active, and an aggregated prion state [*PSI*<sup>+</sup>] with impaired translation termination activity (28). These phenotypes are followed thanks to the red color of an intermediate compound associated with the adenine synthesis pathway. When a stop codon is added inside the enzyme *ADE1* (*ade1-14 mutant*) that should transform this red compound into the next one, [*psi*<sup>-</sup>] strains are not able to read through this stop and are seen as red colonies on rich medium and are not able to grow in the absence of adenine. On the other hand, [*PSI*<sup>+</sup>] strains suppress the premature stop codon in *ade1-14*, and thus appear pink or white on YPD (Yeast extract peptone dextrose) medium. Furthermore, they possess the ability to grow on the plate without adenine source (33). Sup35p protein can also acquire infectious conformation in *E. coli*. Its formation is accelerated by the addition Sup35p aggregates, proving that *E. coli* can generate infectious conformations of heterologous fungal prions (34).

Based on these observations, several researchers have developed system for identifying amyloidogenic proteins and modulators of amyloid aggregation in *E. coli*. This cell-based method provides an easy approach to identify amyloidogenic proteins and enables to distinguish between amyloidogenic and non-amyloidogenic variants of a particular protein.

### **1.7. CDAG system in *E. coli***

Curli-dependent amyloid generator (C-DAG) is a biogenesis pathway that relies on the native ability of *E. coli* cells to elaborate amyloid fibers, known as curli. Curli are class of a highly aggregated, major proteinaceous components of the extracellular matrix produced by *E. coli* and *Salmonella enterica* (35). Generally, the role of cell-surface protein filaments in bacteria is to promote colonization of an epithelial surface, exchange of DNA between bacteria or entry into host cells. It is necessary to mention that curli assembly is not the result of protein misfolding. Assembly relies on *E. coli*'s nucleation-precipitation machinery leaded by the products of several curli-specific genes (*csg*) controlled by two differently transcribed operons, *csgDEFG* and *csgBAC*. Among several genes, CsgD is the main regulator of fibers biogenesis and is required for transcription of the *csgBAC* operon. The rest of curli proteins are secreted into the periplasm by the Sec-translocon system, following transportation of the lipoprotein CsgG to the outer membrane. There CsgG oligomerizes into a pore-like structure that is required for secretion of the major subunit CsgA and the minor subunit CsgB. On the cell surface, the two subunits will associate into an amyloid fiber rich in cross- $\beta$  fold (Figure 3). The overexpression of CsgG, in the absence of all other curli factors, enables the efficient secretion of CsgA, but it does not assemble into amyloid fibrils due to the absece of the nucleator CsgB (35).

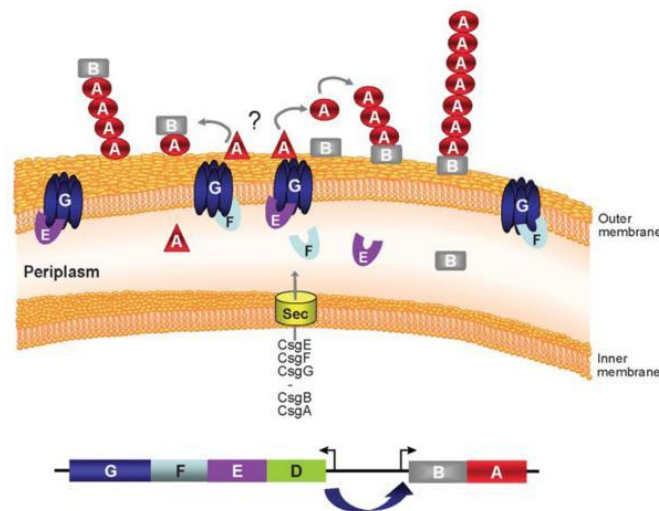


**Figure 3. Schematic diagram of the curli biogenesis** (35). All Csg proteins, except CsgD have Sec-dependent signal sequences allowing their secretion into the periplasm. Lipoprotein CsgG localizes to the inner leaflet of the outer membrane and serve as a curli assembly platform allowing CsgB to nucleate CsgA into highly ordered amyloid fibers.

### **1.7.1. Curli fibers- functional amyloids**

In the year 2002 Chapman et al. proposed the concept of functional amyloids in Science article. Curli fibers as well as other functional amyloids that are produced by different kind of microbes, have biologically important role in biofilm formation. Moreover, they share many distinguishing biochemical and structural characteristics with eukaryotic amyloid fibers (36). Chapman and his coworkers characterized curli fibers produced in *E. coli* biofilms as being biochemically similar to disease-associated amyloid structures (37). The model of curli helped to develop a variety of methods and assays for the identification of microbial amyloids and the environmental components that affect amyloid formation. Additionally, curli are important for surface colonization and interacting with host factors and the host immune system. They are able to interact with Amyloid binding dyes: Congo red (CR) and thioflavin T (ThT), and to resist chemical denaturation with proteases or detergents (e.g., Sodium Dodecyl Sulfate (SDS)). That said, curli formation can be produced in the laboratory by growing on plates supplemented with CR (which binds to curliated whole

cells and is not inhibiting growth) to comparatively quantify whole-cell curliation (37). Since CsgA is the major subunit of curli fibers and because of its capability of *in vitro* self-polymerizing into  $\beta$ -sheet-rich structures, fibers can be examined by using Transmission Electron microscopy (TEM) or by negative-stain electron microscopy (EM). An CsgA mutant would not be able to bind CR or ThT (38). Generally, with TEM or EM, curli polymers can be seen as 4 to 7 nm tangled and amorphous matrix surrounding the bacteria. A disadvantage of mentioned methods is that certain amyloidogenic proteins could be toxic when induced for export.

Researchers worked intensively on comparing the physical properties of pathological amyloid fibers and CsgA fibers. Their results suggest that the essential cross- $\beta$  fold of amyloids is present in curli fibers, most likely as a  $\beta$ -helix structure (39).

## 2. AIM OF THE WORK

The main aim of the work is to prove that gut microbiota encodes for proteins with prion-like domains with the potential to influence human proteins aggregation and, in this way, the development of diseases.

Specifically, in this study, I studied 12 protein candidates that contain a putative amyloid core sequence; selected computationally and *in vitro* for their ability to form amyloid aggregates. The work collected in this study is based on test, in two different microorganisms, that the amyloid cores of these 12 proteins can lead the formation of amyloid aggregates and the cell-to-cell transmission of the aggregated conformation. The two models and experiments done are:

- i) Exploit the curli amyloid fibrils system that sustains the biofilm in *Escherichia coli*, to test that the amyloid cores encoded in the gut microbiota are able to lead the formation of amyloid fibrils in a bacterial model
- ii) Exploit the Sup35p prion system, that regulates translation termination in *Saccharomyces cerevisiae*, to test the ability, of the amyloid cores, to propagate between cells the amyloid aggregated conformation



### 3. MATERIALS AND METHODS

#### 3.1. Putative prion-like peptides

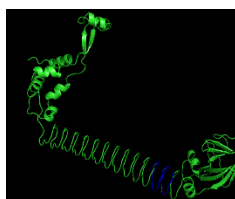
All peptides used in this work were acquired from Peptide Synthesis Facility, Department of Experimental and Health Sciences, University Pompeu Fabra (UPF), Barcelona. Twelve putative prion-like peptides have been found by analyzing the whole proteome of the gut microbiome using PAPA, PLAAC and pWALTZ algorithms (40). They were detected in gut microbiome and most of them are isolated from proteome of gram-positive bacteria (e.g. *Coprococcus comes*, *Roseburia* sp., *Eubacterium* sp. etc.). Those peptides that has been proved to have tendency of amyloid fibrils formation (Table 1, Figure 4) were tested in *E. coli* and *S. cerevisiae* models. To select the protein candidates to study in the unicellular models (C-DAG system in *E. coli* and Sup35p in *S. cerevisiae*), the receiving laboratory classified the sequences present in the gut microbiome proteome accordingly to the scores measured by PAPA, PWALTZ and PLAAC. A protein was considered a putative prion-like if it was predicted to have scores above the threshold of at least two algorithms (PAPA >0.05; pWALTZ >73.55; PLAAC PRDscore >0). After obtaining a final list of prion-like candidates the physicochemical properties and functions collected in UniProt database (41) were also analyzed. Overall, the optimal parameters for the protein candidates were:

- i) sequences should have scores above the threshold of all three algorithms
- ii) proteins located at the membrane/classified by UniProt as uncharacterized should be avoided
- iii) amyloid-forming core should contain at least 20% Qs/Ns
- iv) predicted prion-like regions (from PAPA or PLAAC) and the amyloid forming core (from pWALTZ) should colocalize in the same sequence stretch

**Table 1. List of chosen amyloids forming peptides (1-12) with prion core sequence and short description.**

Simple name	Prion core	Uniprot name	Short description
P1	NTGDYNTGYNTG DYNTGYYN	D4JQH0	Pentapeptide repeats (8 copies)
P2	MQAAFNFNNRRY QDAINVLN	C0B555	DnaJ domain protein
P3	HANEGNVNQYNN SYQNTNSYS	D4KZ46	Trypsin-like serine proteases typically periplasmic contain C- terminal PDZ domain
P4	MDNNYYNNNNNN NTNSNSNYN	C0FUS6	Trypsin
P5	RSGNYVFLANSTN RYQGNYYN	E7GXS5	penicillin-binding protein 1A
P6	YQQALNVLSRIQN RNAQWYYL	C9L6N5	DnaJ domain protein
P7	SSVYWLNSVNENN NNKSYYIS	M3SJI9	putative vacuolating cytotoxin
P8	GNNNNSVISFNQT NFNQGTYN	M5YJZ4	putative vacuolating cytotoxin
P9	GYVQSSYGQNQFQ NSQYGSYQ	F5LFB6	putative RNA-binding protein FUS
P10	SYSSANNYGYGS NYNYSYSA	F0HUU2	aggregation promoting factor
P11	STGYSDLNSTYNQ SALINQIG	G9Y7N7	curlin associated repeat-containing domain protein
P12	GQQGEYQNQQMG YQGQQYGYQ	L1QLH8	toxic anion resistance protein TelA

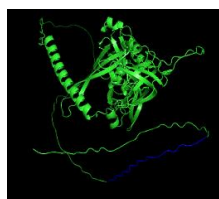
Peptide 1



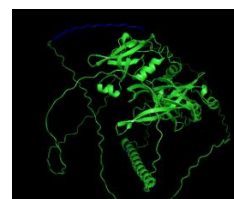
Peptide 2



Peptide 3



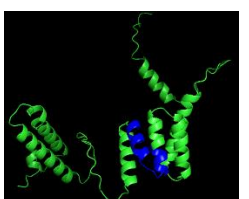
Peptide 4



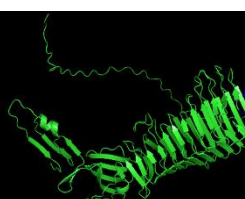
Peptide 5



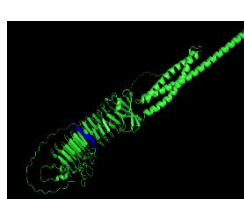
Peptide 6



Peptide 7



Peptide 8



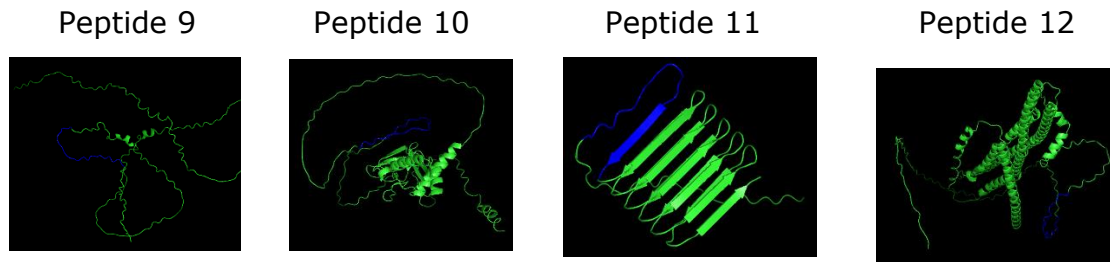


**Figure 4. Models of amyloid forming core peptides (1-12) tested in this work.** All of them are organized as intermolecular  $\beta$ -sheet rich structures except for P1 which consists of random  $\beta$ -turns. Their sequence contains 21 aa residues that were cloned in appropriate plasmids and transformed to conclude on their prionic potential *in vivo*. Every peptide has been verified with sequencing.

### 3.2. *Escherichia coli* system

#### 3.2.1. Strains, growth condition and cultivation

The experiments were based on two different strains of *E. coli* obtained from Ann Hochschild laboratory. The main reporter strain was VS39 which is derivative of MC1601 strain, a naturally competent strain for the formation of amyloids. VS39 was deleted for the curli genes (CsgA, CsgB, and CsgC) and contains a plasmid that directs the Isopropyl  $\beta$ -D-1-thiogalactopyranoside (IPTG)-inducible overproduction of CsgG. Each of the two strains used in this work contains a pExport vector that directs the synthesis of two variants of Sup35p with different lengths, under an IPTG inducible promoter. One plasmid (pVS72) has Sup35NM and the other one (pVS105) just Sup35M. In both cases, the prion protein was fused to two essential elements of the curli system: (i) a SecA-dependent secretion signal (CsgA<sub>ss</sub>) and (ii) a CsgG targeting sequence. These plasmids also carried a constitutively transcribed gene that provided resistance to carbenicillin.

Cells were made competent before use, following the protocol (42) and were grown in Luria Broth medium (LB) with the chloramphenicol (the resistance enclosed in VS39). Chloramphenicol was used at 25  $\mu$ g/mL (final conc.) during cultivation for maintaining the plasmid encoding CsgA. LB

medium was prepared following the protocol (43) while additional components (e.g. antibiotics or inducers) were added after the medium was autoclaved and cooled down to room temperature (22 °C).

LB agar plates for *E.coli* transformations, as well as Congo red (CR) plates were prepared following the protocol (40). Later, transformants were cultured and plated on an inducing medium containing CR to determine the colony color phenotype.

### **3.2.2. Plasmid isolation, purification, and transformation**

First step was to insert the DNA sequence of twelve peptides of interest that are encoding for the proteins. The insertion of the gene of interest was performed by using two partially complementary oligonucleotides and Polymerase Chain Reaction (PCR) on Thermofischer Scientific® Thermal cycle machine. Amplification has been proceeded by using a PCR Touch-down method (Table 2). This approach differs from standard method in the second (Annealing) step. Here, the temperature was reduced, one degree each cycle from 65°C to 55°C. High-Fidelity Q5® DNA Polymerase has been used for extension of the DNA. For every peptide, the reaction mix was prepared following the instructions provided by the manufacturer (19).

**Table 2. Touch-down PCR program used in cloning of gene of interest.**

Cycle 1	60s 98 °C (at least 4 min. because the region is long and rich in GC)
Cycle 2	(10 times reducing temperature one degree each cycle from 65-55 °C) 30s 95 °C 15s 65-55 °C 4 min 72 °C
Cycle 3 (repeated 30 times)	30s 95 °C 20s 58 °C / 20 s 62 °C 4 min 72°C
Cycle 4	5 min 72 °C

In order to separate, analyze and identify plasmid DNA, next step was gel electrophoresis with 0,7% (w/v) agarose gel and transformation in

competent MC1061 *E. coli*. Agarose gel was prepared by solving 0,35g of agarose in 50ml of 0.5xTBE (Tris/Borate/EDTA) buffer. Staining was performed with 2,5µl of SYBR Green intercalator. Then, a volume of 3µl of DNA ladder and 5µl of samples have been loaded and the gel has been running at 90V for approximately 20 minutes. Afterwards, the gel was viewed with an ultraviolet (UV) transilluminator. Images of the gels were obtained with a Gel Doc 1000 device from BioRad. If strong DNA bands with a size of 500bp were obtained, samples were cut with Dpn1 enzyme in order to remove all metilated DNA and to proceed with transformation. Cutting with Dpn1 is an important step in the targeted mutagenesis method using PCR because it eliminates the parent strand, since it was metilated during its amplification in *E. coli*. The parent strand does not contain the mutation and its presence decreases the transformation efficiency of the desired DNA. Competent MC1061 cells were transformed with all peptides using heat shock method (44) and plated on LB agar plate supplemented with 100 ug/ml carbenicillin. After overnight incubation at 37 °C, colonies were picked with a loop and placed in a colony PCR mixture (45) as a template for examining the presence of vectors with insert, using standard 2% (w/v) agarose gel electrophoresis. Next day plasmid DNA was extracted from the overnight cultures using Thermo Scientific™ GeneJET™ Plasmid Mini Kit and following the instructions provided by the manufacturer. Plasmid DNA of every peptide was sent on sequencing to prove if the gene of interest was inserted in the right way. It was ensured that Open Reading Frame (ORF) includes all necessary elements such as the CsgA<sub>ss</sub>, the sequence encoding the 3-alanine linker and the gene of interest. DNA sequencing has been performed through the services of the company Sistemas Genómicos S.L. of Paterna, Valencia, using the Sanger method. The samples came from DNA extractions performed on cells transformed with the mutated DNA.

The next step required was the transformation of competent VS39 cells with the pExport plasmid containing the gene of interest. Transformed cells were plated on LB agar supplemented with 100 µg/ml carbenicillin and

25 µg/ml chloramphenicol and put on incubation at 37 °C, 250 rpm, for 12 hours. Colonies that have grown were saved in 15% glycerol at -80 °C. From the glycerol, I examined phenotypic assay based on curli aggregates affinity to bind CR.

### **3.2.3. Congo red (CR) binding assay**

In order to induce the production of amyloid fibers I grew the different strains on solid LB medium with CR. First comparison was dependent on the color between colonies grown on solid LB medium with CR containing 100 µg/ml carbenicillin, 25 µg/ml chloramphenicol and inducers (0.2 % w/v L-arabinose and 1 mM IPTG - also called "inducing plate") for both CsgG and the target fusion protein and colonies grown on solid non-inducing LB plate with CR (supplemented only with antibiotics). When they are grown on CR-containing nutrient plate, curled whole cells bind CR and deplete the dye from the agar. LB plate with only antibiotics has been used as a control. *E. coli* strain VS39 transformed with peptide of interest were cultured overnight in LB medium with carbenicillin and chloramphenicol at 37 °C. Next day, turbidity has been measured with Cary 300 spectrophotometer (Varian), as the reduction in light transmission due to the presence of particles in a suspension. The residual transmitted light was quantified as optical density (OD). In that way it was possible to find out a number of *E. coli* in overnight suspension. OD was adjusted at 0,01 for every culture. Fresh cultures were then incubated on shaker for additional 3 hours at 37 °C. After the incubation period, I put drops of 5 µl at each plate, listed above. Colonies have been left to grow during 3 days at room temperature (25 °C). Color of colonies transformed with plasmid containing peptide insertion have been compared with positive and negative control as well as with Δ1-40 in order to conclude about curli biogenesis.

To measurable the amount of CR bound, the cells were extracted from the plates with Phosphate Buffered Saline (PBS). These samples were employed to measure both, CR absorbance at 510 nm, and amyloid fibril visualization by Transmission electron microscopy (TEM). For CR

measurement, the same concentration of cells was centrifugated and incubated for 1 hour in ethanol: acetone (80:20) medium. The absorbance of between 400-600 nm was measured, to observe how CR spectrum shifts to larger wavelengths when it binds amyloid fibrils. The spectrum of the ethanol: acetone alone was acquired as a blank to subtract background. Later, the results were analyzed in Excel.

#### **3.2.4. Transmission electron microscopy (TEM)**

TEM JEOL 1400 was employed to assess the presence and morphology of amyloid fibers in cell strain. Samples were incubated for at least 48 hours before negative staining. Volume of 10 $\mu$ L of dilution was placed onto carbon-coated copper microscopy grids and incubated for 5 min. Then, freshly prepared uranyl acetate 1% (w/v) was added for 1 min to enable staining of samples. After washing the grid in deionized water, samples have been stored for examination for the presence of fibers using a Transmission electron microscope. ImageJ program was used to measure the length/width of the fibrils and mean value was taken to compare curli amyloids of tested peptides with positive control.

### **3.3. Analysis of prion behavior in *Saccharomyces cerevisiae***

Plasmid based assay used in this work was developed in 2001 by Parham and his colleagues (46). Briefly, Sup35p is essential for the cell viability and the deletion of its chromosomal copy need to be compensated by expressing the wild-type *SUP35* gene; this was done in a *URA3* centromeric (*CEN*) plasmid (pYK810). The strain used in this assay was derived from 74D-694 *MATa*, *ade1-14UGA*, *trp1-289*, *his3 $\Delta$ -200*, *ura3-52*, *leu2-3,112 sup35::loxP* [pYK810]). The N-terminal Sup35p modified quimeres (where the first 40 residues are replaced with 21 residues peptides) are expressed from a new plasmid bearing a *HIS3* selection marker (a pUCK plasmid). After introduction of the centromeric pUCK plasmids with the *SUP35*-chimeres into yeast, cells were forced to lose the pYK810 plasmid by growing in 5-fluoro-orotic acid (5-FOA)-containing medium. 5-FOA is toxic for the yeast

cell when they are expressing Ura3p, and consequently stimulate the loss of the original pYK810 vector. By this means, plasmid shuffling has been implemented, and therefore it was possible to avoid the expression of the original Sup35p and to have exclusively the expression of the new N-terminal modified chimera. Although, the non-sense suppressor assay could be carried at this point (with the endogenous expression of Sup35p-chimeres), the overexpression significantly improves the sensibility of this assay. Afterwards, cells were transformed with an episomal vector (pESC-GFP) able to overexpress the corresponding NM-chimeres (but only with the NM domain and without the functional C-domain) fused to the green fluorescent protein GFP in order to induce aggregation and increase the  $[PSI^+]$  phenotype (Figure 5). Thus, yeast cells were assessed for the *ade1-14* non-sense suppressor assay, where  $[PSI^+]$  colonies will be expected to show white or pink colour with Ade<sup>+</sup> phenotype, while  $[psi^-]$  colonies will be red and Ade<sup>-</sup>. Because of expression of NM-chimeres fused to GFP, the aggregation has been followed by fluorescent microscopy by the formation of fluorescent foci (Figure 11).



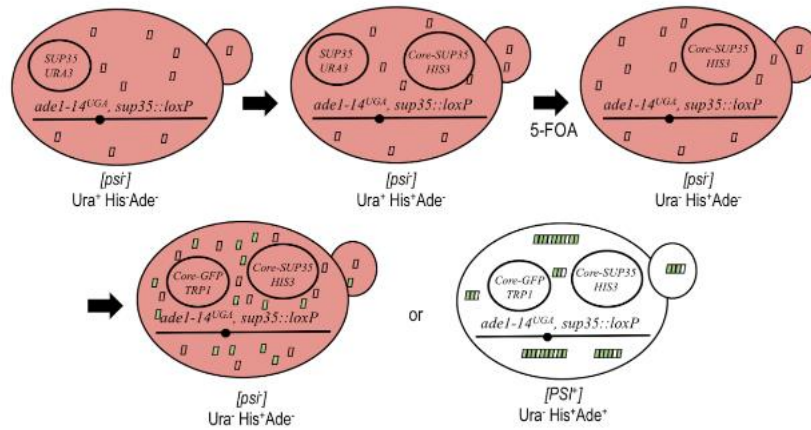


**Figure 5. Schema of functional substitution of Sup35p by Core-Sup35 chimeras.** Yeast cells containing a premature stop codon in *ade1-14* gene and having a soluble Sup35p terminator factor (empty rectangles) expressed from the *URA3-CEN*-expression plasmid show red phenotype depending on adenine supplementation. These cells were transformed with a *HIS3-CEN*-plasmid expressing the chimera Core-Sup35, and the *URA3*-vector was counter-selected with FOA. The unique source of Sup35p is now the P9-chimera. Next, transformation with a new plasmid capable to overexpress the fusion protein Core-GFP induced the aggregation of Core-Sup35p. Cells with aggregated Core-Sup35p are white and independent on adenine supplementation. Moreover, they show punctate fluorescence foci (green rectangles) (47).

### 3.3.1 Endogenous expression of Sup35p chimeres and plasmid shuffling

The centromeric vector pUCK1620 bearing the promoter and complete sequence of *SUP35* gene was used as positive control (hereafter NM). For the negative control, sequence codifying 1-40 residues in the N-terminal of Sup35p was deleted by the IVA method (48) (primers used were Fw: CACTAGCAACAAAAAATGTCTGCAGGTGGGTACTACCAAATTACC and Rv: AGACATTTTTTGTGCTAGTGGGCAGATATGGATGTTATTCCGAGC). After that, the sequence codifying for peptide 9 was inserted in the same way (primers used were Fw: TCAAAACCAATTCCAAACTCTCAATACGTTCTTACCAAGCAGGTGGGTACTACCAAATTACC; and Rv: AGTTTTGGAATTGGTTTTGACCATAGGAGGATTGAACGTAACCAGACATTTTTTGTGCTAGTGGGC). The same program already indicated in Table 2 was used

but with shortened denaturation time (1 min). Once, peptide 9 was inserted in NM domain (NM-P9) and the 1-40 codifying region of NM was deleted (NM  $\Delta$ 1-40), all three plasmids were digested with DpnI and transformed into *E. coli* MC1061. Plasmidic DNA was extracted and was verified by sequencing. Yeast cells were, then, transformed and colonies bearing the plasmids were selected by growing in synthetic dextrose medium without histidine (SD His<sup>-</sup>): 0.67% yeast nitrogen base without amino acids, 0.2% glucose, 0.2% bacto-agar, supplemented with amino acids but without histidine). Colonies were transferred to SD His<sup>-</sup> 5-FOA plates (SD His<sup>-</sup> plates supplemented with 0.1% 5-fluoroorotic acid). Afterwards, they were replica-plated in chemically defined culture medium plates without histidine (SD His<sup>-</sup> or SD His<sup>-</sup>Ura<sup>-</sup>). Colonies growing in both plates were discarded, and those growing only in SD His<sup>-</sup> were selected as the colonies that have lost the original pYK810 vector (Figure 5).

### **3.3.2. Overexpression of NM-P9 fused to GFP**

In order to increase the efficiency of prion conversion, the yeast colonies selected in the previous step, were transformed with a multicopy plasmid able to overexpress either the NM, the NM  $\Delta$ 1-40 or the NM-P9 domain fused to the green fluorescent protein (GFP). With that aim, NM domains were amplified by PCR (Table 3.) and introduced into pESC-GFP vector by recombination (48). A sequence codifying for the 10 residues "GSAGSAAGSG" was included as a linker between NM domains and GFP. Primers used here were Fw:GAATTCAACCCTCACTAAAGGGCGGCCGCACTAGTACATCCATATCTGCCC ACTAGCAAC and Rv: ACCAGAACCAGCAGCAGAACCGGCGGAACCAAACATATCGTTAACAACCTTCGTC ATCCACTTC. Vector pESC-GFP has the 2  $\mu$ m replication origin, GAL10 promoter and *URA3* as selective marker (49). PCR products were treated with DpnI and co-transformed with the vector into *E. coli*. Plasmidic DNA extracted from the positive clones was verified by sequencing and

transformed into yeast following the PEG/LiAc method (50) (Figure 6 steps b and c).

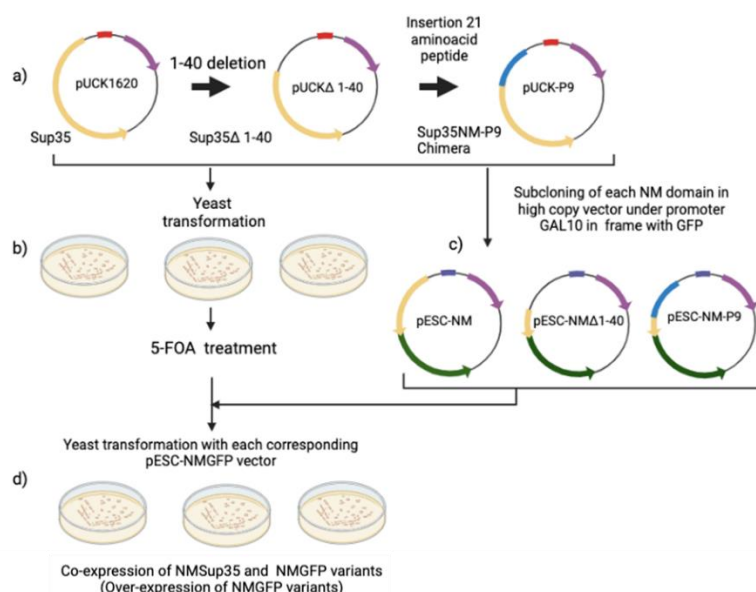


**Figure 6. Overview of steps for the endogenous expression of NM-Sup35p and overexpression of NM-GFP chimeres.** **a)** pUCK vectors allow the expression of the different forms of NM Sup35 at physiological level. NM  $\Delta$ 1-40 was obtained by deletion of the corresponding sequence in pUCK1620 vector. After that, peptide 9 sequence was introduced in pUCK  $\Delta$ 1-40. **b)** All three plasmids were transformed into yeast and the expulsion of pYK810 vector was induced with 5-FOA. **c)** NM domains were introduced into a pESC-GFP vector fused to GFP; **d)** Each yeast strain was transformed with the corresponding pESC-NM chimera, for its overexpression. In this way, when overexpressed NM-GFP aggregates, it will also drag the NM Sup35p expressed at physiological level, therefore increasing the prion phenotype.

**Table 3. PCR volumes of ingredients and program steps for pESC-NMGFP colony verification.**

1 PCR reaction (volume)	Program
12.6 ml water	Cycle 1: 2 min 95°C
2 ml 10X DreamTaq Buffer	Cycle 2: 30s 95°C
0.4 ml dNTPs 10 mM	Cycle 3 (repeated 30 times): 30s 65°C

0.8 ml Fw-Sup-GFP/ RV-GFP2 primer mixture (25 mM each)	Cycle 4: 1 min 72°C
0.2 ml Dream Taq DNA pol	

### **3.3.3. Phenotypic assay**

Firstly, precultures with each yeast transformants were prepared in synthetic medium with raffinose and without uracil and histidine (SRaf His<sup>-</sup>Ura<sup>-</sup>) medium and incubated at 30 °C and vigorous agitation for 3 days. Then, 1 ml of the previous preculture was inoculated into 20ml of the same medium but supplemented with galactose (SRafGal His<sup>-</sup>Ura<sup>-</sup>) for inducing the expression of NM-GFP chimera under the inducible GAL promoter. After three days of incubation, OD600 nm has been adjusted in the range of 0,1-0,7 by preparing 1 ml of 1/10 dilution. Mediums were prepared as 20 ml of SD -Ade and 10 ml of SD +Ade. All cultures were set as OD600 ~ 1 in SD without adenine. To obtain red/white phenotype; 100µl of the 1/1000 and 1/10,000 dilutions were plated in pre-warmed ¼ YPD plates and incubated at 30 °C for 2-3 days. Red phenotype was checked after 3-5 days since red color is developing at 4 °C (Figure 10a).

Moreover, analysis of aggregation was also analyzed by fluorescence microscopy. 1 ml of SRaf His<sup>-</sup>Ura<sup>-</sup> pre-cultures grown for three days were inoculated into SRafGal His<sup>-</sup>Ura<sup>-</sup>, and grown at 30 °C, for 24 hours. After washing cells, by spinning and resuspension of the cell pellet in PBS, 40 µl of cell suspension was transferred to a 96-well plate and incubated for 5 min to allow the cell attachment. The remaining liquid has been discharged by draining with the pipette and repeated two more washing in PBS. Finally, 100 µl of PBS was added, and cells were examined by fluorescence microscopy (Figure 11b).

### **3.3.4. Western blot analysis**

Preculture was prepared in the same way as for testing the aggregation in phenotypic assay. The culture was spin-down in a falcon,

resuspended in 200  $\mu$ L of Tris-EDTA (TE) buffer and transferred to a pre-weighted Eppendorf. Cells were spined for 1 min, and the liquid was drained with the pipet. The pellet was weighted, and Yeast Protein Extraction Reagent (YPER) was added in ratio 2.5 (v/w). The mixture was incubated 20 min at room temperature at 500 rpm. Later, supernatant (soluble fraction) was taken to a new tube and the pellet was resuspended in the same volume of loading buffer. Next step included mixing of each soluble fraction and pellets with loading buffer (4x), followed by incubation at 95 °C for 5 minutes. Samples were loaded into a 10% SDS-PAGE and run for 45 minutes at 200 V. Rainbow marker, Amersham TM was loaded as a reference. The gel was transferred to immobilon P membrane, which was blocked with 0.1% Tris-buffered saline (TBST) and 5% powdered milk. Primary antibody was IgG antiGFP (1/7500; over-night) while peroxidase conjugated anti-rabbit IgG (BioRad) (1/3000) served as secondary antibody. Finally, gel was viewed with chemiluminescent detector (Figure 10c).

## 4. RESULTS

In the experimental work first 40 amino acids of N domain were deleted from Sup35 protein (hereafter  $\Delta 1-40$ ). Every peptide (P1-12) sequence contained 21 amino acids that were inserted using primers in the deleted region. Substitution of fragments in the place of the first 40 amino acids of Sup35p was used to probe aggregation propensity of these domains and to examine how the mutation affects it.

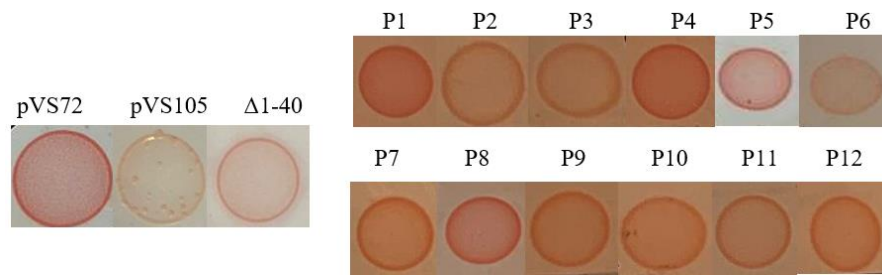
In the *E. coli* model, Sup35p was fused to the CsgA signal sequence (CsgA<sub>ss</sub>). When a plasmid containing Sup35p protein NM (hereafter pVS72) is introduced in *E. coli*, Sup35p is able to produce extracellular amyloid fibrils. Thus, in this work, pVS72 was used as a positive control and a plasmid with just Sup35 M domain (pVS105) served as a negative one. The amyloidogenicity of the twelve Sup35p variants has been tested with C-DAG system in *E. coli*. Apart from this, peptide 9 was tested in the yeast model using the above-mentioned adenine method (Figure 5).

### 4.1. Production of curli

#### 4.1.1. Congo red phenotypic assay- plates

Colonies of VS39 transformed with plasmid carrying peptide inserts (P1-12) have grown on all plates after 72 hours of incubation. Three controls were also tested. Sign of positive curli production on CR plate containing inducers was shown as a bright red colony with a strongly red edge, while negative control that is not able to induce amyloid formation in same conditions was binding less on CR dye, so the colonies had opaque white color with paler edges (Figure 7a). The positive control (pVS72) drop had a brighter redness than the one of negative control or the deleted ( $\Delta 1-40$ ) mutant of Sup35p, which did not exhibit significant CR binding.

a)



b)

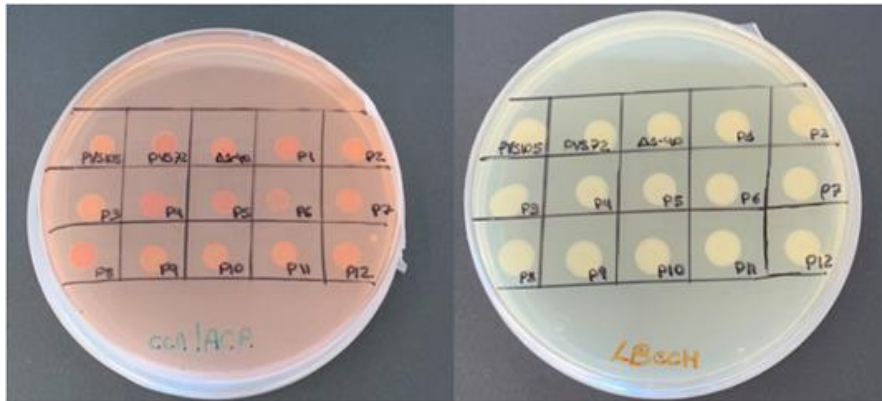


**Figure 7. Results of phenotype testing amyloidogenicity of 12 protein variants on the plates. a)** Difference in curli production between positive and negative control, compared to truncated version of Sup35p and Core-Sup35 fusions. Observed on the inducing plate. **b)** LB plate containing CR, showing that different strains have different ability to bind this dye (left) and LB plate without inductors supplementation used to check the growth (right).

Results show that all peptides had a high capability of producing curli fibrils. Although, colonies of P4, P5 and P8 had the most reddish edge on the inducible plate (Figure 7a), similar to positive control. The rest of colonies show slightly lower ability of producing amyloids, but there is still noticeable difference in color when compared to negative control or deleted version. For those peptides that are shown bright red, colonies were extremely attached to the plate, which indicates the formation of a strong biofilm. Importantly, colonies growth was similar between all peptides, except for P6. These cells showed less growth, indicating toxicity associated with the Sup35p variant containing the P6 peptide. Results obtained on the plate basis were compared to results obtained from the phenotypic assay based on binding CR in liquid.

#### 4.1.2. Congo red phenotypic assay- liquid

To obtain a quantitative value of the CR binding to the amyloid fibrils produced for the different *E. coli* strains, the CR was extracted and measured. After obtaining the absorbance scan of every CR extraction (Figure 8.), the highest absorbance was present for pVS72, while the lowest CR binding has pVS105, and the deleted version of Sup35p (D1-40). Binding results of the C-DAG system containing the amyloid core peptides were based on the red shift in absorbance at 510nm. Observations are presented as bar plot of CR absorbance at 510nm for every peptide regarding negative control. Peptide 4 showed the highest capacity for binding CR among all peptides, almost as positive control, followed by P9 and P6. The peak of CR absorbance has been observed at 510nm. So, results obtained from the CR extraction match only partially with the results obtained on the CR plates.

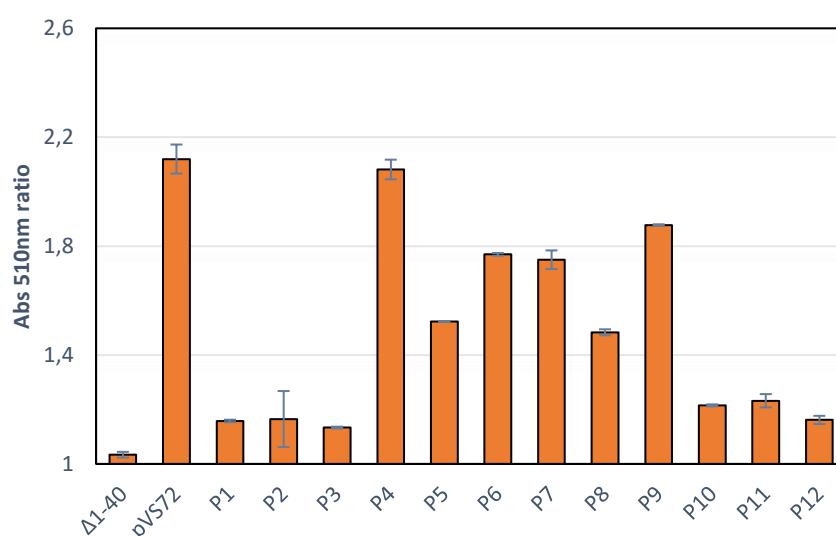


**Figure 8. CR absorbance at 510 nm for all *E. coli* strains tested.** Peptide 4 binds CR in highest amount, almost as positive control. The rest of the peptides are found in between positive and negative control where P5-8 show higher binding than P1-3 and P10-12. The absorbance of CR binding for every peptide was measured three times, and plots present a mean of three measurements. Error bars show standard error calculated in Excel.



#### **4.1.3. Curli fibers characterization**

By employing TEM, negative-stain micrographs of transformed VS39 grown on LB inducible plates (at 25 °C for 72 hours) were obtained (Figure 9). All 12 cells expressing Sup35p variants containing the peptide fragments derived from the gut microbiota have fibrillar aggregates with different abundance. On the negative control grids, only *E. coli* cells were seen (Figure 9b,c), while positive control provides dense curli structures localized on the cell surface (Figure 9a).

Furthermore, it can be seen in the images that curli amyloids are interwoven and structured as a tangled mass of linear, surface-associated fibers with a diameter of few micrometers. Moreover, amyloid fibers for all peptides were seen as unbranched structures. Curli morphology produced by the amyloid core peptides is quite similar to those formed by the positive control. In general, almost all peptides produced longer fibrils than positive control, except P3,5 and 6 (Table 4). The largest fibrils were found in those strains expressing the peptide 7 ( $l=7,45\ \mu\text{m}$ ) and 12 ( $l=5,01\ \mu\text{m}$ ) (Figure 9 j,o ). On the other hand, the shortest ( $l=0,62\ \mu\text{m}$ ) and thinnest ( $w=0,036\ \mu\text{m}$ ) fibrils were seen in the environment of *E. coli* bearing P6. They were far less abundant in comparison to positive control and other peptides. All other peptides were similar in width (mean value= $0,18\ \mu\text{m}$ ) compared to positive control with  $0,21\ \mu\text{m}$  of width.

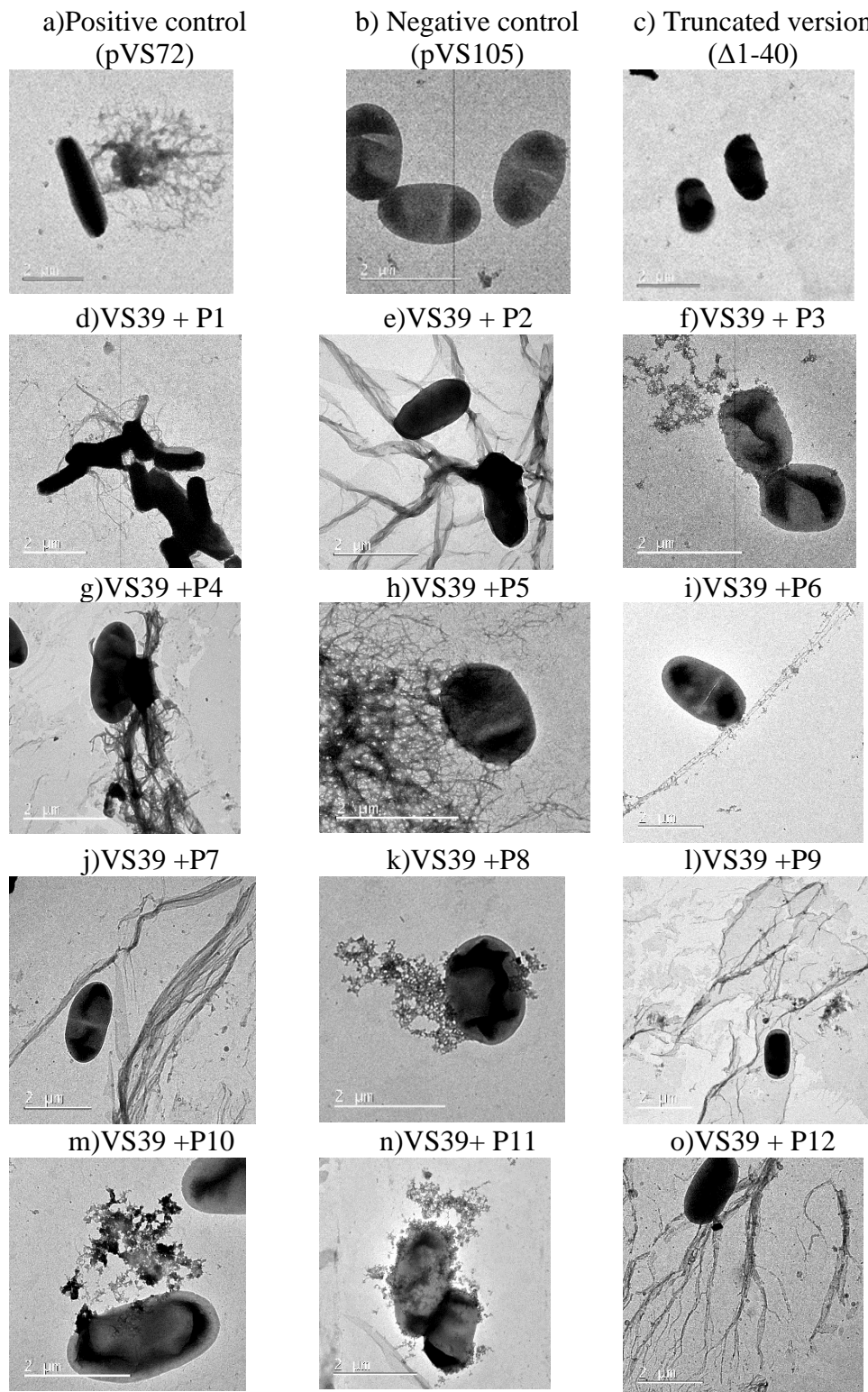


**Figure 9. TEM images of curli production by *E. coli* after insertion of 21 amino acids of chosen prion-like peptides. a)** Control of positive curli formation **b,c)** Bacteria not expressing curli **d-o)** Curli formation due to core-amyloid forming peptide. *E. coli* were stained negatively and are shown as dark dots. The scale bar represent 2μm.

**Table 4. Length and width of curli fibers formed by positive control and 12 tested peptides.** Measurements were done by using Fiji-Image J program. Fibrils were measured five times and score is represented as a mean value.

Peptide	Length (l)/ $\mu\text{m}$	Width (w)/ $\mu\text{m}$
pVS72	1,21	0,21
P1	1,36	0,13
P2	1,64	0,25
P3	0,99	0,075
P4	2,28	0,21
P5	0,89	0,091
P6	0,62	0,036
P7	7,45	0,22
P8	1,21	0,18
P9	2,99	0,21
P10	2,89	0,18
P11	1,62	0,26
P12	5,01	0,22

## 4.2. Analysis of peptide 9 prion behavior in the yeast model

This assay was performed firstly with the positive and negative controls (NM and NM  $\Delta$ 1-40 respectively) and one chosen peptide, the peptide 9 (NM-P9). As was previously explained in detail (see material and methods section), the two NM controls and the one modified with peptide 9, were expressed at physiological level in form of full Sup35 protein (with their NM and C-terminal domains).

In order to increase the prion conversion phenotype, the different NM domains were also fused to GFP and overexpressed. This is expected to trigger the aggregation on all NM containing proteins inside the cell: both the different NM-GFP fusions and their corresponding Sup35p version. NM-GFP overexpression was under control of the inducible GAL10 promoter, which is highly repressed in presence of glucose, and induced by galactose. Therefore, yeast cells were induced to express NM-GFP fusions for 3 days, in presence of galactose, and plated on ¼ YDP plates (containing glucose) for prion conversion analysis. As stated before, aggregation of Sup35p allowed bypass the non-sense mutation in the *ade1-14* gene, and consequently, cells stopped accumulating a red pigment and become pink, or white, depending on the degree of aggregation ( $[PSI^+]$  colonies), while non-prion colonies remain red ( $[psi^-]$  colonies). This phenotype is also transmitted to the progeny, so, we can observe different colonies colors. For the NM; the 96% of colonies were prion positive  $[PSI^+]$ , while in the case of NM  $\Delta$ 1-40 it was just the opposite, with 99% of colonies showing a non-prion  $[psi^-]$  phenotype. For the NM containing the peptide 9, 76% of colonies showed  $[PSI^+]$  phenotype manifested in white/pink coloration and here they overcounts non-prionic ones (24%) (Figure 10a and b).

The expression of the NM-GFP fusions was also verified in yeast extracts by western-blotting and immunodetection with anti-GFP antibody. The expected 68 kDa band was observed, with some lower bands probably derived from protein degradation. For NM, the protein was mainly detected

in the insoluble fraction, while NM  $\Delta$ 1-40 and NM-P9 were detected in both, soluble and insoluble fractions (Figure 10c).

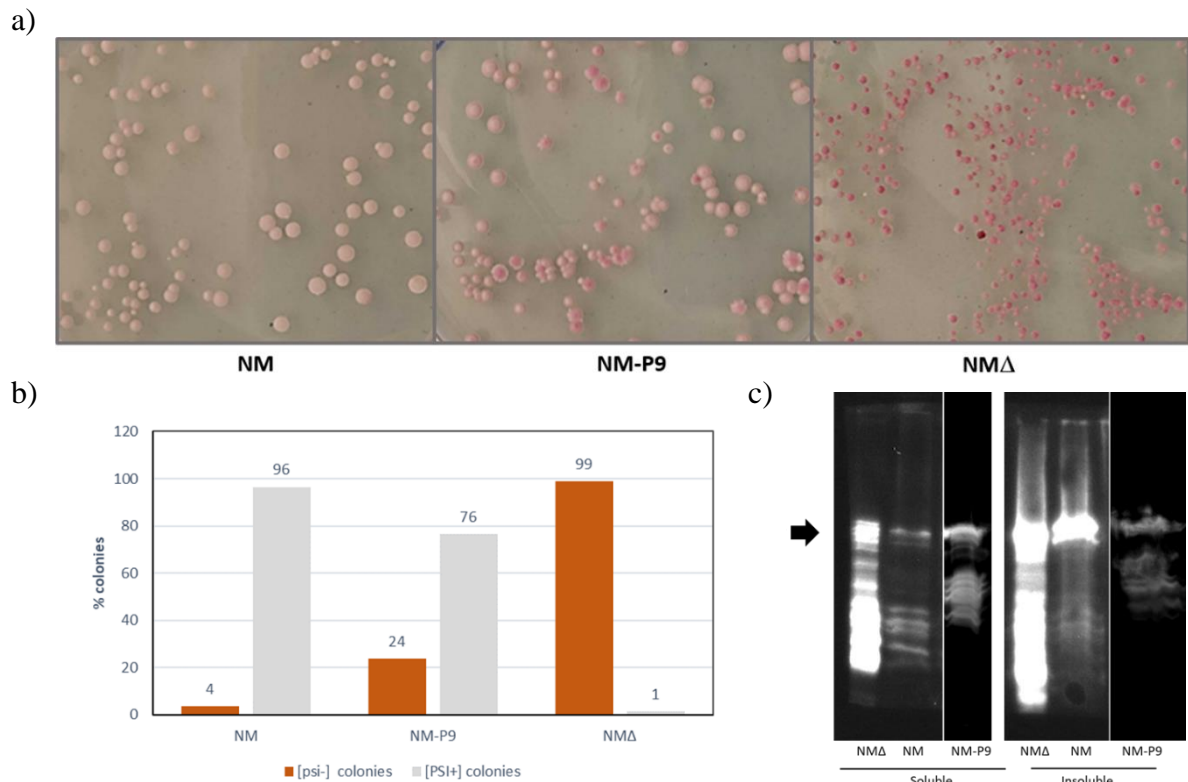


**Figure 10. Analysis of the prion behavior and expression of the NM-GFP fusions.** **a)** Red and white/pink colonies shown in 1/4 YPD plates; **b)** Graphic representation of the percentage of prion and non-prion colonies showed in each case. Colonies were counted from the plates and results were processed in Excel; **c)** Analysis of the expression of the NM-GFP fusions by western-blot and immunodetection with anti-GFP antibody. Soluble and insoluble fractions were analyzed. The arrow indicates the 68 kDa band corresponding to the NM-GFP fusions. NM $\Delta$ , refers the deleted NM  $\Delta$ 1-40 form.

Moreover, overexpression of NM-GFP fusions allowed *in vivo* analysis of the NM aggregation. Yeast cells expressing original NM domain showed foci formation, indicating intracellular aggregation; while no focus were shown in the 1-40 deleted NM mutant, were GFP seems to be mainly soluble and distributed all over the cell. Concerning the NM bearing peptide 9, it made foci like in the original Sup35 NM domain, but also some ring-like and curved aggregates can be observed in few cells (Figure 11).

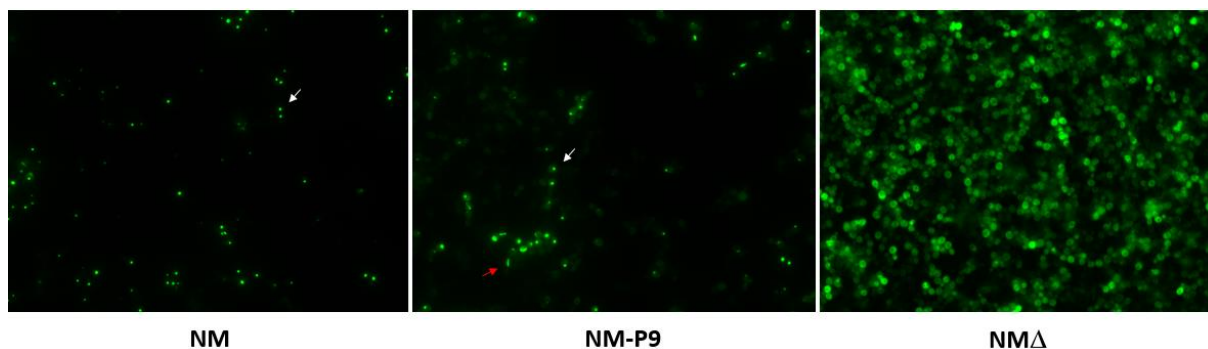


**Figure 11. Analysis by fluorescent microscopy of NM-GFP fusions.** The NM corresponding domain is indicated under the picture. The white arrow indicates a foci, while the red arrow signals a curved aggregate. Original magnification was 400x. NM $\Delta$ , refers the deleted NM  $\Delta$ 1-40 form.

## 5. DISCUSSION

### 5.1. Production of curli

To determine whether the amyloid cores of twelve selected peptides could seed A $\beta$ 40, focus of this thesis has been on their aggregation ability. Start for these experiments was in the fact that first 40 amino acids of the Sup35p PrD are required for prion formation. If that sequence is deleted and inserts of amyloid core are cloned in the right place, *E. coli* will export and produce curli amyloids, while yeast cells will accumulate amyloid aggregates in form of insoluble [PSI<sup>+</sup>]. Therefore, this work achieves the substitution of fragments in the place of the first 21 residues to probe the aggregation propensity of these domains.

Likewise, it is known that all amyloid fibers cause a red shift when mixed with CR meaning that more binding for CR is associated with a higher presence of amyloid aggregates. The CR binding results suggested that every examined peptide had a different capability for curli production. Furthermore, all peptides showed fibrillar structure under the TEM. Results obtained from TEM can be associated to phenotypic assay observations. The best matches in the three provided methods are seen for P4 and P9. Other results differ between methods. For example, P6 showed the lowest CR binding on the plate, while CR binding in liquid was sufficient to conclude about amyloid formation. For P12, plate results were better than ones obtained in liquid. Finally, microscope analysis confirmed that all 12 tested amyloid cores are able to produce curli fibrils but combining of these two phenotypic methods opened a space for improving clarity and specificity of A $\beta$  aggregates accumulation, even there is still a need for calibration of steps involved in clarification process.

By selecting colonies that stained a bright shade of red, I confirmed that chosen peptides have ability to assemble as amyloid fibers. After observing of red color intensity (liquid and pellet) and taking in account TEM results; it is obvious that NM-P4 among others has the highest potentiality to interfere A $\beta$ 40 aggregation in *E. coli* model. All other peptides had similar

CR binding affinity with absorptions in between positive and negative control (Figure 8). On the other hand, peptide 6 had the most interesting background since there were only few of *E. coli* cells when the sample was analyzed under the TEM. Small number of bacteria, with certain amount of curli in their environment, point out on potential toxicity of core forming amyloid toward bacteria cells. Moreover, NM-P6 produced fibers had a different structure and were the shortest in comparison to others. Structural differences between each peptide induced curli, take place in order and orientation of amino acid residues inside the  $\beta$ -sheet. Molecular structure of curli is not strictly dependent on peptide sequence, so  $\beta$ -structures that are forming amyloid fibers will also differ among peptides due to variant aggregation conditions or mutations inside sequences. One suggestion for P6 toxicity is that: due to the sequence insertion of P6, C-DAG system is exporting pre-fibrillar/oligomeric entities of amyloid type. As mentioned above, there are strong evidence provided in the literature that explain how intermediate structures as protofibrils are able to interact with the cell membrane consequently causing cell death by permeabilizing the membrane. This may be the reason why VS39 strain containing NM-P6 sequence is growing less on the plate. Length and width of examined P6-fibrils confirms theory of their toxicity depending on their size and easier ability to diffuse through tissue. It seems like prefibrillar entities may be even more pathogenic than mature fibrils. Moreover, researchers pointed out that some functional amyloids, as in this case curli amyloids formed by P6, may act as cytotoxins, killing vulnerable neighboring cells and providing a linker to the classical disease-associated amyloids.

Results obtained from the part examining bacteria system, indicate that heterologous core-forming amyloid proteins derived from human gut straightway acquire the amyloid fold when secreted via the *E. coli* curli export system. They are matching with similar researches carried out on different bacteria species (35,51). It is notable that regulation of curli subunit polymerization in *E. coli* may offer wide access to the formation of



eukaryotic amyloids or amyloids that accumulate in human's brain. Even if they differ from the CNS amyloids in their primary structure, they share similarities inside tertiary structure and their exposure in the gut may affect the immune system, consequently reinforcing immune response to endogenous production of neuronal amyloid. Few publications (24,26) already pointed out increasement in neuronal alpha-synuclein ( $\alpha$ -syn) deposition in rats exposed to curli amyloids produced by *E. coli* in both the gut and brain. Those rats have developed microgliosis and astrogliosis and increased expression of TLR2, IL-6, and TNF unlike rats exposed to bacteria without the ability to produce curli. Consequences are unrolling due to process called molecular mimicry where bacterial amyloids function as prion proteins and influence cross-seeding, in which one amyloidogenic protein e. g. curli or A $\beta$  cause another; e.g, host proteins with a different primary structure; to adopt pathogenic  $\beta$ -sheet conformation.

## **5.2. Transmission of the aggregated conformations in yeast**

On other hand, the prion-like phenomenon [*PSI*<sup>+</sup>] of *Saccharomyces cerevisiae* has opened a window into molecular basis of amyloid propagation and specificity. In this work, I achieved to adjust a method for testing the amyloid properties of selected peptides in the yeast model. Many variation of this screening method have been reported, but most of them were focusing on expression of prion-like domains and substituting the N domain of Sup35p at physiological level (52). This approach, usually implies the screening of a large number of colonies due to the low rate of prion conversion at physiological level of expression. Recently, new methods overexpressing the NM domain in order to increase prion conversion have been reported (53). Approximation presented here, has been adapted to test the prionic behaviour of the selected peptides.

It is desirable to repeat that, inserted peptides in QNR region would act as the core of the amyloid fibers of Sup35p while the OPR is essential for continued propagation of the [*PSI*<sup>+</sup>] state. Tests were processed for the peptide 9, which is proved to be amyloidogenic in the previous assays.

These results proved that the deletion of the first 40 residues of Sup35p almost abolished prion conversion of Sup35p, while its substitution by peptide 9 is able to compensate that loss in large extent (Figure 11). This indicates that peptide 9 is functionally equivalent to the deleted region, and proves its ability to nucleate and therefore support prion transmission of Sup35p. Nevertheless, prion conversion was higher with the intact NM domain (96%) than with NM-P9 chimeric domain (76%). This could indicate that its nucleative activity is less strong than in the original region. Also, we cannot rule out that the size of the region (40 residues exchanged by 21) could have something to do with that decrease in prion conversion. In the same way, analysis by western-blot and immunodetection of the NM-GFP chimeres showed that for the original NM domain most of the protein remains in the insoluble fraction, while NM-P9 is in both fractions, soluble and insoluble. Moreover, by fluorescent microscopy both NM and NM-P9 showed the presence of foci, indicating again, *in vivo* aggregation; while the N domain, deleted in its first forty residues, remains soluble and distributed all over the cell (Figure 11). Yet, for the NM-P9 domain few cells show a curved ribbon or a ring-like fluorescent assemblies. It has been described that prion induction implicates a process of maturation, in which NM-GFP first assemble into rings and ribbons that transition later into dots (or foci). These rings and ribbons are composed of long interrupted bundles of fibers, while the dots contain highly fragmented fibers (54). This indicates that NM-P9 is delayed in its prion maturation with respect to NM, which would also be consequence of decrease in nucleative activity, referred to the one of NM.

All in all, this work proved the strength of used assay, which may be implemented for the study of other potential peptides in the future. Peptide 9 has been selected for examination in both unicellular organisms because of its interesting functions and already known features of two devastating neurodegenerative diseases, Amyotrophic lateral sclerosis (ALS) and frontotemporal dementia (FTD). P9 is classified as RNA-binding protein

(RBP) FUS (fused in sarcoma) and its aggregates have been found in neurons and glial cells of the postmortem brain and spinal cord of patients that suffered from above mentioned diseases (55). Furthermore, researchers have concluded about the accumulation of aggregated Sup35p in the prion-containing cells and its association with cell death (e.g. neuron cells) (56). If we consider the fact that misfolded and potentially aggregating proteins are usually accumulated during aging, hypothesis of aging promotion of prion-like pathologies can be easily derived. Here, P9 showed the ability to nucleate Sup35p and support its prion transmission in yeast cells. That said, it can be suggested that other peptides which are proved to produce curli amyloids in *E. coli* with the same or higher capability, will provide equivalent results in yeast model. These findings may contribute to wider understandings of how A $\beta$  plaques are produced and how microbiota and prion-like proteins derived from it, are an important factor in manipulation of gut-brain axis toward neurodegeneration.

## 6. CONCLUSION

From all provided results obtained by testing CDAG-system in *E. coli*, evaluating phenotypic changes and amyloid aggregation in the yeast model it is possible to conclude the following:

- The amyloid core corresponding to the first 40 amino acids of the Sup35p prion can be substituted by an amyloid core sequence of just 21 amino acids.
- The 12 amyloid cores obtained from gut microbiota, when introduced into the C-DAG system and using the Sup35p prion as a common protein body, are able to form curli amyloid fibrils with different efficiency.
- When the amyloid cores obtained from gut microbiota are introduced in Sup35p, they can recover the protein prion behavior.
- The two exploited microbial models showed that the 12 candidate proteins encoded in the gut microbiome are able to lead the formation of amyloid aggregates and to transmit the aggregated conformation.
- These two properties support the fact that proteins may have the potential to influence other proteins' aggregation, such as the human ones, and, in this way, affect the development of diseases

## 7. LITERATURE

1. Turnbaugh PJ, Ley RE, Hamady M, Fraser-Liggett CM, Knight R, Gordon JI. The Human Microbiome Project. *Nat* 2007 449:7164 [Internet]. 2007 Oct 17 [cited 2022 Aug 1];449(7164):804–10. Available from: <https://www.nature.com/articles/nature06244>
2. Vuong HE, Yano JM, Fung TC, Hsiao EY. The Microbiome and Host Behavior. *Annu Rev Neurosci* [Internet]. 2017 Jul 7 [cited 2022 Jun 4];40:21. Available from: [/pmc/articles/PMC6661159/](https://pmc/articles/PMC6661159/)
3. Hardy JA, Higgins GA. Alzheimer's disease: The amyloid cascade hypothesis. *Science* (80- ) [Internet]. 1992 [cited 2022 May 25];256(5054):184–5. Available from: <https://www.science.org/doi/abs/10.1126/science.1566067>
4. Alzheimer's Association | Alzheimer's Disease & Dementia Help [Internet]. [cited 2022 May 25]. Available from: <https://www.alz.org/>
5. Goedert M, Clavaguera F, Tolnay M. The propagation of prion-like protein inclusions in neurodegenerative diseases. *Trends Neurosci* [Internet]. 2010 Jul 1 [cited 2022 May 25];33(7):317–25. Available from: <http://www.cell.com/article/S016622361000055X/fulltext>
6. López De La Paz M, Serrano L. Sequence determinants of amyloid fibril formation. *Proc Natl Acad Sci U S A* [Internet]. 2004 Jan [cited 2022 May 29];101(1):87–92. Available from: <https://pubmed.ncbi.nlm.nih.gov/14691246/>
7. Karran E, Mercken M, Strooper B De. The amyloid cascade hypothesis for Alzheimer's disease: an appraisal for the development of therapeutics. *Nat Rev Drug Discov* 2011 10:9 [Internet]. 2011 Aug 19 [cited 2022 May 25];10(9):698–712. Available from: <https://www.nature.com/articles/nrd3505>
8. Chiti F, Dobson CM. Protein Misfolding, Amyloid Formation, and Human Disease: A Summary of Progress Over the Last Decade. <https://doi.org/10.1146/annurev-biochem-061516-045115> [Internet]. 2017 Jun 27 [cited 2022 May 25];86:27–68. Available from: <https://www.annualreviews.org/doi/abs/10.1146/annurev-biochem-061516-045115>
9. 3D PFV: 5KK3 [Internet]. [cited 2022 May 25]. Available from: <https://www.rcsb.org/3d-sequence/5KK3?assemblyId=0>
10. Verma M, Vats A, Taneja V. Toxic species in amyloid disorders: Oligomers or mature fibrils. *Ann Indian Acad Neurol*. 2015 Apr 1;18(2):138–45.
11. Alberti S, Halfmann R, King O, Kapila A, Lindquist S. A systematic survey identifies prions and illuminates sequence features of prionogenic proteins. *Cell* [Internet]. 2009 Apr 3 [cited 2022 May 25];137(1):146–58. Available from: <https://pubmed.ncbi.nlm.nih.gov/19345193/>
12. Uptain SM, Lindquist S. Prions as Protein-Based Genetic Elements. <http://dx.doi.org/10.1146/annurev.micro56013002100603> [Internet]. 2003 Nov 28 [cited 2022 May 26];56:703–41. Available from:

<https://www.annualreviews.org/doi/abs/10.1146/annurev.micro.56.013002.100603>

13. Sabate R. When amyloids become prions. *Prion* [Internet]. 2014 May 1 [cited 2022 May 25];8(3):233–9. Available from: <https://pubmed.ncbi.nlm.nih.gov/24831240/>
14. Fändrich M, Dobson CM. The behaviour of polyamino acids reveals an inverse side chain effect in amyloid structure formation. *EMBO J* [Internet]. 2002 Nov 1 [cited 2022 Jun 3];21(21):5682–90. Available from: <https://pubmed.ncbi.nlm.nih.gov/12411486/>
15. Haerty W, Brian Golding G. Low-complexity sequences and single amino acid repeats: Not just “junk” peptide sequences. *Genome*. 2010 Oct;53(10):753–62.
16. Tetz G, Tetz V. Prion-like Domains in Eukaryotic Viruses. *Sci Rep* [Internet]. 2018 Dec 1 [cited 2022 May 25];8(1). Available from: <https://pubmed.ncbi.nlm.nih.gov/29895872/>
17. Stefani M. Protein misfolding and aggregation: new examples in medicine and biology of the dark side of the protein world. *Biochim Biophys Acta* [Internet]. 2004 Dec 24 [cited 2022 May 29];1739(1):5–25. Available from: <https://pubmed.ncbi.nlm.nih.gov/15607113/>
18. Dasari M, Espargaro A, Sabate R, Lopez Del Amo JM, Fink U, Grelle G, et al. Bacterial Inclusion Bodies of Alzheimer’s Disease  $\beta$ -Amyloid Peptides Can Be Employed To Study Native-Like Aggregation Intermediate States. *ChemBioChem* [Internet]. 2011 Feb 11 [cited 2022 May 29];12(3):407–23. Available from: <https://onlinelibrary.wiley.com/doi/full/10.1002/cbic.201000602>
19. PCR Using Q5® High-Fidelity DNA Polymerase (M0491) | NEB [Internet]. [cited 2022 Jun 5]. Available from: <https://international.neb.com/protocols/2013/12/13/pcr-using-q5-high-fidelity-dna-polymerase-m0491>
20. Petra AI, Panagiotidou S, Hatziagelaki E, Stewart JM, Conti P, Theoharides TC. Gut-microbiota-brain axis and effect on neuropsychiatric disorders with suspected immune dysregulation. *Clin Ther* [Internet]. 2015 May 5 [cited 2022 May 25];37(5):984. Available from: [/pmc/articles/PMC4458706/](https://pubmed.ncbi.nlm.nih.gov/25458706/)
21. Heijtz RD, Wang S, Anuar F, Qian Y, Björkholm B, Samuelsson A, et al. Normal gut microbiota modulates brain development and behavior. *Proc Natl Acad Sci U S A* [Internet]. 2011 Feb 15 [cited 2022 Jun 4];108(7):3047–52. Available from: [www.pnas.org/cgi/doi/10.1073/pnas.1010529108](http://www.pnas.org/cgi/doi/10.1073/pnas.1010529108)
22. Sudo N, Chida Y, Aiba Y, Sonoda J, Oyama N, Yu XN, et al. Postnatal microbial colonization programs the hypothalamic–pituitary–adrenal system for stress response in mice. *J Physiol* [Internet]. 2004 Jul 1 [cited 2022 Jun 4];558(1):263–75. Available from: <https://onlinelibrary.wiley.com/doi/full/10.1113/jphysiol.2004.063388>
23. Hu X, Wang T, Jin F. SCIENCE CHINA Alzheimer’s disease and gut microbiota. 2016;59(10):1006–23.
24. Zhao Y, Dua P, Lukiw WJ, Lukiw WJ, Bollinger Professor Of Alzheimer’s O.

- Microbial Sources of Amyloid and Relevance to Amyloidogenesis and Alzheimer's Disease (AD) HHS Public Access. *J Alzheimers Dis Park*. 2015;5(1):177.
25. Zhao Y, Lukiw WJ. TREM2 signaling, miRNA-34a and the extinction of phagocytosis. *Front Cell Neurosci*. 2013 Aug 29;0(AUG):131.
  26. Friedland RP. Mechanisms of molecular mimicry involving the microbiota in neurodegeneration. *J Alzheimers Dis* [Internet]. 2015 [cited 2022 May 30];45(2):349–62. Available from: <https://pubmed.ncbi.nlm.nih.gov/25589730/>
  27. Zajkowski T, Lee MD, Mondal SS, Carbajal A, Dec R, Brennock PD, et al. The Hunt for Ancient Prions: Archaeal Prion-Like Domains Form Amyloid-Based Epigenetic Elements. *Mol Biol Evol* [Internet]. 2021 May 1 [cited 2022 May 25];38(5):2088–103. Available from: <https://pubmed.ncbi.nlm.nih.gov/33480998/>
  28. Liebman SW, Derkatch IL. The Yeast [PSI+] Prion: Making Sense of Nonsense \*. *J Biol Chem* [Internet]. 1999 Jan 15 [cited 2022 May 31];274(3):1181–4. Available from: <http://www.jbc.org/article/S0021925819882182/fulltext>
  29. Ter-Avanesyan MD, Kushnirov V V., Dagkesamanskaya AR, Didichenko SA, Chernoff YO, Inge-Vechtomov SG, et al. Deletion analysis of the SUP35 gene of the yeast *Saccharomyces cerevisiae* reveals two non-overlapping functional regions in the encoded protein. *Mol Microbiol* [Internet]. 1993 Mar 1 [cited 2022 May 31];7(5):683–92. Available from: <https://onlinelibrary.wiley.com/doi/full/10.1111/j.1365-2958.1993.tb01159.x>
  30. Marchante R, Rowe M, Zenthon J, Howard MJ, Tuite MF. Structural Definition Is Important for the Propagation of the Yeast [PSI+] Prion. *Mol Cell* [Internet]. 2013 Jun 6 [cited 2022 Jul 16];50(5):675. Available from: </pmc/articles/PMC3679450/>
  31. Santoso A, Chien P, Osherovich LZ, Weissman JS. Molecular Basis of a Yeast Prion Species Barrier. *Cell*. 2000 Jan 21;100(2):277–88.
  32. Liu JJ, Sondheimer N, Lindquist SL. Changes in the middle region of Sup35 profoundly alter the nature of epigenetic inheritance for the yeast prion [PSI+]. *Proc Natl Acad Sci U S A* [Internet]. 2002 Dec 10 [cited 2022 Jul 6];99(SUPPL. 4):16446–53. Available from: <https://www.pnas.org>
  33. Garrity SJ, Sivanathan V, Dong J, Lindquist S, Hochschild A. Conversion of a yeast prion protein to an infectious form in bacteria. *Proc Natl Acad Sci U S A* [Internet]. 2010 Jun 8 [cited 2022 Jun 3];107(23):10596–601. Available from: [www.pnas.org/cgi/doi/10.1073/pnas.0913280107](http://www.pnas.org/cgi/doi/10.1073/pnas.0913280107)
  34. Sabaté R, Espargaró A, Saupe SJ, Ventura S. Characterization of the amyloid bacterial inclusion bodies of the HET-s fungal prion. *Microb Cell Fact* [Internet]. 2009 Oct 28 [cited 2022 Jun 4];8(1):1–10. Available from: <https://microbialcellfactories.biomedcentral.com/articles/10.1186/1475-2859-8-56>
  35. Barnhart M, microbiology MC-A review of, 2006 undefined. Curli biogenesis


- and function. ncbi.nlm.nih.gov [Internet]. [cited 2022 Jun 4]; Available from: <https://www.ncbi.nlm.nih.gov/pmc/articles/pmc2838481/>
36. Olsén A, Jonsson A, Normark S. Fibronectin binding mediated by a novel class of surface organelles on *Escherichia coli*. *Nature*. 1989;338(6217):652–5.
  37. Chapman MR, Robinson LS, Pinkner JS, Roth R, Heuser J, Hammar M, et al. Role of *Escherichia coli* Curli Operons in Directing Amyloid Fiber Formation. *Science* [Internet]. 2002 Feb 2 [cited 2022 Jun 1];295(5556):851. Available from: </pmc/articles/PMC2838482/>
  38. Blanco LP, Evans ML, Smith DR, Badtke MP, Chapman MR. Diversity, biogenesis and function of microbial amyloids. *Trends Microbiol* [Internet]. 2012 Feb [cited 2022 Jun 4];20(2):66. Available from: </pmc/articles/PMC3278576/>
  39. Shewmaker F, McGlinchey RP, Thurber KR, McPhie P, Dyda F, Tycko R, et al. The Functional Curli Amyloid Is Not Based on In-register Parallel  $\beta$ -Sheet Structure. *J Biol Chem*. 2009 Sep 11;284(37):25065–76.
  40. LB agar + carbenicillin plates. *Cold Spring Harb Protoc* [Internet]. 2008 Aug 1 [cited 2022 Jun 2];2008(8):pdb.rec11374. Available from: <http://cshprotocols.cshlp.org/content/2008/8/pdb.rec11374.full>
  41. Bateman A, Martin MJ, O'Donovan C, Magrane M, Apweiler R, Alpi E, et al. UniProt: a hub for protein information. *Nucleic Acids Res* [Internet]. 2015 Jan 28 [cited 2022 Jul 28];43(Database issue):D204–12. Available from: <https://pubmed.ncbi.nlm.nih.gov/25348405/>
  42. Li X. RbCl Super Competent Cells. *BIO-PROTOCOL*. 2011;1(11).
  43. LB (Luria-Bertani) liquid medium. *Cold Spring Harb Protoc* [Internet]. 2006 Jun 1 [cited 2022 Jun 2];2006(1):pdb.rec8141. Available from: <http://cshprotocols.cshlp.org/content/2006/1/pdb.rec8141.full>
  44. Bacterial Transformation Workflow–4 Main Steps | Thermo Fisher Scientific - HR [Internet]. [cited 2022 Aug 1]. Available from: <https://www.thermofisher.com/hr/en/home/life-science/cloning/cloning-learning-center/invitrogen-school-of-molecular-biology/molecular-cloning/transformation/bacterial-transformation-workflow.html>
  45. DreamTaq DNA Polymerases | Thermo Fisher Scientific - ES [Internet]. [cited 2022 Jun 5]. Available from: [https://www.thermofisher.com/es/es/home/brands/thermo-scientific/molecular-biology/thermo-scientific-pcr/thermo-scientific-pcr-enzymes-master-mixes/hot-start-dna-polymerases-master-mixes-thermo-scientific/dreamtaq-dna-polymerase.html?ef\\_id=Cj0KCQjwqPGUBhDwARIsANNwjV7rOB28bg3K7ogccEuni3JNlwyE\\_HsejV6AnspFCzIYs45B4Zz9RXUaAhn5EALw\\_wcB:G:s&s\\_kwcid=AL!3652!3!560796270939!p!!g!!dreamtaq-polymerase&cid=bid\\_mol\\_pch\\_r01\\_co\\_cp1358\\_pjt0000\\_bid00000\\_0se\\_gaw\\_bt\\_pur\\_con&gclid=Cj0KCQjwqPGUBhDwARIsANNwjV7rOB28bg3K7ogccEuni3JNlwyE\\_HsejV6AnspFCzIYs45B4Zz9RXUaAhn5EALw\\_wcB](https://www.thermofisher.com/es/es/home/brands/thermo-scientific/molecular-biology/thermo-scientific-pcr/thermo-scientific-pcr-enzymes-master-mixes/hot-start-dna-polymerases-master-mixes-thermo-scientific/dreamtaq-dna-polymerase.html?ef_id=Cj0KCQjwqPGUBhDwARIsANNwjV7rOB28bg3K7ogccEuni3JNlwyE_HsejV6AnspFCzIYs45B4Zz9RXUaAhn5EALw_wcB:G:s&s_kwcid=AL!3652!3!560796270939!p!!g!!dreamtaq-polymerase&cid=bid_mol_pch_r01_co_cp1358_pjt0000_bid00000_0se_gaw_bt_pur_con&gclid=Cj0KCQjwqPGUBhDwARIsANNwjV7rOB28bg3K7ogccEuni3JNlwyE_HsejV6AnspFCzIYs45B4Zz9RXUaAhn5EALw_wcB)
  46. Parham SN, Resende CG, Tuite MF. Oligopeptide repeats in the yeast protein



- Sup35p stabilize intermolecular prion interactions. *EMBO J* [Internet]. 2001 May 5 [cited 2022 Jul 16];20(9):2111. Available from: [/pmc/articles/PMC125439/](https://pmc/articles/PMC125439/)
47. Fernández MR, Pallarès I, Iglesias V, Santos J, Ventura S. Formation of Cross-Beta Supersecondary Structure by Soft-Amyloid Cores: Strategies for Their Prediction and Characterization. *Methods Mol Biol* [Internet]. 2019 [cited 2022 Aug 2];1958:237–61. Available from: [https://link.springer.com/protocol/10.1007/978-1-4939-9161-7\\_12](https://link.springer.com/protocol/10.1007/978-1-4939-9161-7_12)
  48. García-Nafría J, Watson JF, Greger IH. IVA cloning: A single-tube universal cloning system exploiting bacterial In Vivo Assembly. *Sci Reports* 2016 61 [Internet]. 2016 Jun 6 [cited 2022 Aug 2];6(1):1–12. Available from: <https://www.nature.com/articles/srep27459>
  49. Manual I. pESC Yeast Epitope Tagging Vectors. *researchgate.net* [Internet]. [cited 2022 Jul 16]; Available from: [https://www.researchgate.net/profile/Christopher-Fernandez-Prada/post/Any\\_advice\\_for\\_yeast\\_coexpression\\_vectors/attachment/59d626a6c49f478072e9affb/AS%3A272179919294484%401441904158502/download/217451.pdf](https://www.researchgate.net/profile/Christopher-Fernandez-Prada/post/Any_advice_for_yeast_coexpression_vectors/attachment/59d626a6c49f478072e9affb/AS%3A272179919294484%401441904158502/download/217451.pdf)
  50. Gietz RD, Schiestl RH. High-efficiency yeast transformation using the LiAc/SS carrier DNA/PEG method. *Nat Protoc* [Internet]. 2007 Feb [cited 2022 Jul 16];2(1):31–4. Available from: <https://pubmed.ncbi.nlm.nih.gov/17401334/>
  51. Römling U, Bian Z, Hammar M, Sierralta WD, Normark S. Curli fibers are highly conserved between *Salmonella typhimurium* and *Escherichia coli* with respect to operon structure and regulation. *J Bacteriol* [Internet]. 1998 [cited 2022 Jul 18];180(3):722–31. Available from: <https://journals.asm.org/doi/10.1128/JB.180.3.722-731.1998>
  52. Chandramowliswaran P, Sun M, Casey KL, Romanyuk A V., Grizel A V., Sopova J V., et al. Mammalian amyloidogenic proteins promote prion nucleation in yeast. *J Biol Chem* [Internet]. 2018 Mar 2 [cited 2022 Aug 2];293(9):3436–50. Available from: <https://pubmed.ncbi.nlm.nih.gov/29330303/>
  53. Paul KR, Molliex A, Cascarina S, Boncella AE, Taylor JP, Ross ED. Effects of Mutations on the Aggregation Propensity of the Human Prion-Like Protein hnRNPA2B1. *Mol Cell Biol* [Internet]. 2017 Apr 15 [cited 2022 Aug 2];37(8). Available from: <https://pubmed.ncbi.nlm.nih.gov/28137911/>
  54. Tyedmers J, Treusch S, Dong J, McCaffery JM, Bevis B, Lindquist S. Prion induction involves an ancient system for the sequestration of aggregated proteins and heritable changes in prion fragmentation. *Proc Natl Acad Sci U S A* [Internet]. 2010 May 11 [cited 2022 Aug 2];107(19):8633–8. Available from: <https://www.pnas.org/doi/abs/10.1073/pnas.1003895107>
  55. King OD, Gitler AD, Shorter J. The tip of the iceberg: RNA-binding proteins with prion-like domains in neurodegenerative disease. *Brain Res*. 2012 Jun 26;1462:61–80.
  56. Inge-Vechtomov S, Zhouravleva G, Chernoff YO, Inge-Vechtomov SG, Zhouravleva GA. Biological Roles of Prion Domains.

<http://dx.doi.org/10.4161/pri.145059> [Internet]. 2007 [cited 2022 Jul 6];1(4):228–35. Available from: <https://www.tandfonline.com/doi/abs/10.4161/pri.1.4.5059>

## 8. CURRICULUM VITAE

 europass

**Iva Tić**

Date of birth: 10/07/1998 | **Nationality:** Croatian | **Gender:** Female | (+385) 953361655 | [iva.tic1@gmail.com](mailto:iva.tic1@gmail.com) |  
Rijeka, Croatia

● **EDUCATION AND TRAINING**

01/02/2022 – 01/07/2022 – Cerdanyola del Vallès, Barcelona, Spain  
**PRACTICAL TRAINING AT "SELF-ORGANIZATION IN BIOLOGICAL SYSTEMS" LAB** – Department of Biochemistry and Molecular Biology, UAB

Testing in unicellular models (yeast and bacteria) the aggregation potential and prion behavior of proteins expressed by the microbiota from human gut. This included: molecular cloning, fluorescent microscopy and culture of yeast and bacteria strains.

01/02/2022 – 01/07/2022 – Barcelona, Spain  
**ERASMUS EXCHANGE** – Autonomous University of Barcelona

Molecular Biology of Cancer, Nanobiotechnology  
<https://www.uab.cat/>

2020 – CURRENT – Ul. Radmile Matejčić 2, Rijeka, Croatia  
**MASTER'S DEGREE IN DRUG RESEARCH AND DESIGN** – University of Rijeka, Department of Biotechnology

"Toxicology and pharmacology", "Drug Development and Registration", "Natural Compounds and their use in Pharmacology", "Antitumor and antiviral drugs", "Colloids", "Protein Research Methods"  
Western blot method, Mass spectrometry  
<https://www.biotech.uniri.hr/hr/>

2017 – 2020 – Ul. Braće Branchetta 20/1, , Rijeka, Croatia  
**BACHELOR'S DEGREE IN SANITARY INGENEERING** – University of Rijeka, Faculty of Medicine

"Biology", "Physiology with pathophysiology", "Basics of anatomy and histology" "Microbiology and Parasitology", "Microbiology of food and water", "Life under the microscope", "Molecular Medicine and Biotechnology", "Chemistry and Biochemistry"...

**Thesis:** Francisella novicida - cytopathic effect on a macrophages and amoebae cells  
<https://www.medri.uniri.hr/en/>

2013 – 2017 – Vukovarska 58, Croatia  
**HIGH SCHOOL DIPLOMA** – Natural Science and Graphics School Rijeka

● **PUBLICATIONS**